B lifetime measurement using exclusively reconstructed hadronic B Decays[1]

1 Introduction

We measure the $B^{\pm}$ and $B^0/\overline{B}^0$ lifetimes as well as their ratio using events that contain one fully reconstructed B candidate. The data sample consists of 7.4 fb^{-1} of e^+e^- collisions collected near the $\Upsilon(4S)$ by the *BABAR* detector in 2000.
We fully reconstruct clean hadronic two-body decay modes to hidden and open charm. Full reconstruction of the B mesons benefits from powerful constraints that can be used to distinguish charged Bs from neutral Bs. The individual lifetimes of the two species can be measured separately, rather than an average "B lifetime".
An inclusive technique is used to reconstruct the decay vertex of the second B in an event, and the lifetimes are determined from the distance between the decay vertices of the two B mesons. This novel method, developed for use at an asymmetric B Factory, deals with event topologies similar to those in measurements of time-dependent *CP* asymmetries. In the latter analyses, the distance between the two decay vertices is used to follow the time-dependence. The measurement of B lifetimes using this novel technique is a significant step towards *CP* violation analyses.

The simple spectator quark decay model predicts equal lifetimes for charged and neutral B mesons. Differences in the lifetimes can arise, e.g. from non-spectator effects like weak annihilation and W exchange. Because the b quark is significantly heavier than the c quark, the expected difference of the two B meson lifetimes is much smaller than that observed for their charmed counterparts ($\tau_{D^+}/\tau_{D^0} \simeq 2.5$ [1]). Various models, e.g. [2, 3], give different predictions for a lifetime difference of up to 20 %. At present, the world averages for the B lifetimes and their ratio are [4, 1]: τ_0=1.548±0.032 ps; τ_-=1.656±0.025 ps; τ_-/τ_0=1.062±0.029. These numbers are the combined results from several experiments at SLC, LEP and CDF. The precision is not yet sufficient to make a meaningful distinction between different models. The *BABAR* experiment will eventually reach an interesting level of statistical precision for results obtained with a different method and different systematic errors.

The method used to determine the B meson lifetimes is outlined in section 2 and the detector components most relevant to this measurement are reviewed in section 3. B re-

[1]Editors: J.Chauveau, Chih-hsiang Cheng, D.Kirkby, F. Martínez-Vidal, C. Roat and J. Stark.

construction, the candidate selection criteria used and the signal yields are described next (section 4). The measurements of the decay vertices of the two B mesons in each selected event are discussed in section 6. Thorough studies of the resolution on the distance between the two vertices are presented. They are necessary to disentangle the effects of the B lifetimes and the experimental resolution. The fitting procedure used to extract the B lifetimes from our sample of neutral B mesons and our sample of charged B mesons comes next (section 8). The results are given in section 10. Consistency checks are described in section 11 and systematic uncertainties are discussed in section 12.

2 The decay length difference technique

At an asymmetric B Factory the $\Upsilon(4S)$ decay products are Lorentz boosted and fly long enough for their flight paths to be comparable to the experimental resolution. Since no charged stable particles emerge from the $\Upsilon(4S)$ decay point, we determine the B lifetimes from the difference between the decay lengths of the two B mesons in an event.
The z axis of the *BABAR* coordinate system is defined to be parallel to the magnetic field in the solenoid [5]. Suppose the boost of the machine was parallel to the z axis and the B mesons were produced exactly at threshold in $\Upsilon(4S)$ decays. The B momenta in the $\Upsilon(4S)$ rest frame would be zero. Define $z_{\rm rec}$ and $z_{\rm opp}$ as the z coordinates of the decay points of the fully reconstructed and the opposite B, respectively. We call $\Delta z = z_{\rm rec} - z_{\rm opp}$ the signed decay length difference. Under the above assumptions, $|\Delta z|$ is distributed exponentially with an average of $\langle|\Delta z|\rangle = (\beta\gamma)_B c\tau_B = p(4{\rm S})/M(4{\rm S})$. Complications arise from several effects. The axis of the PEP-II beams is tilted by 20 mrad with respect to the z axis [5], and the energies of the beams fluctuate, giving the $\Upsilon(4S)$ momentum a gaussian distribution with a standard deviation of 6 MeV/c [6]. Furthermore, the energy release in the $\Upsilon(4{\rm S}) \to B\overline{B}$ decay makes the B mesons move in the $\Upsilon(4S)$ rest frame. The latter effect has the highest impact on the Δz distribution of our events, but all of these effects are small compared to the experimental resolution on Δz [6].
The topology of the events is sketched in figure 1. It is not drawn to scale. The opening angle between the trajectories of the B mesons is generally non-zero because of the energy release in $\Upsilon(4{\rm S}) \to B\overline{B}$, and it is always smaller than 214 mrad [7]. The flight paths are of the order of 260 μm and the errors on $z_{\rm rec}$ and $z_{\rm opp}$ are usually of the order of 50 μm and 150 μm, respectively.

In the present analysis we work with Δz, i.e. the difference of the projections of the decay paths on the z axis. Therefore we use $(\beta_z\gamma)_B$ instead of $(\beta\gamma)_B$. β is the length of the boost vector $\vec{\beta}$ and β_z is the projection on the z axis. γ describes the time dilatation and is calculated using the full length β. We use $(\beta_z\gamma)_{\Upsilon(4S)}$ as an approximation for $(\beta_z\gamma)_B$. The average boost $\vec{\beta}_{\Upsilon(4S)}$ of the centre-of-mass frame is measured on a run by run basis using 2-prong events [8].
This procedure automatically takes into account a systematic tilt of the beam axis with respect to the z axis. We fully reconstruct one of the two B mesons per event and have a run by run determination of the $\Upsilon(4S)$ momentum. We could therefore take into account the

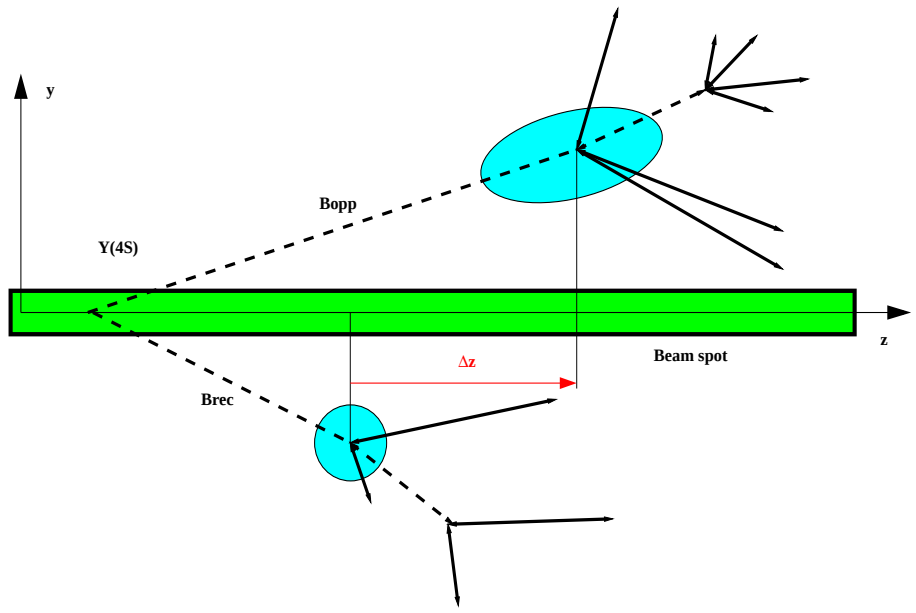

Figure 1: Event topology. The figure is not drawn to scale (see text).

effect of the energy release in $\Upsilon(4\mathrm{S}) \to B\overline{B}$ by calculating $(\beta_z\gamma)_B$ for each B individually, but the systematic error introduced by our approximation is small (see section 12.8). Figure 2 shows the theoretical Δz distribution for two extreme cases: flight direction of the two Bs orthogonal to the z axis in the centre-of-mass frame, and both Bs flying along the z axis in the centre-of-mass frame.

3 Detector and data set

The data used in this analysis were collected with the *BABAR* detector at the PEP-II storage ring in the period January - June, 2000. The total integrated luminosity of the data set is 7.4 fb^{-1} collected near the $\Upsilon(4S)$ resonance and 0.9 fb^{-1} collected 40 MeV below the $\Upsilon(4S)$ resonance (off-resonance data). The corresponding number of produced $B\bar{B}$ pairs is estimated to be 8.4×10^6.

The *BABAR* detector is described elsewhere [9]. For this measurement, the most important subdetectors are the silicon vertex tracker (SVT) and the central drift chamber (DCH) which provide tracking and the electromagnetic calorimeter (EMC) from which photons and π^0s are reconstructed. The charged particle momentum resolution is approximately $(\delta p_T/p_T)^2 = (0.0015\, p_T)^2 + (0.005)^2$, where p_T is in GeV/c. The SVT, with a typical single-hit resolution of 10 μm provides vertex information in both the transverse plane and in z. The precision on charged particle momenta, neutral particle energies and spatial coordinates from the tracking and calorimetry lead to resolutions on invariant masses and other kinematical quantities which allow a clean separation of the complex decay trees we reconstruct (see section 4). Impact parameter resolutions in the transverse plane are $\simeq 50\,\mu$m at high momentum, and

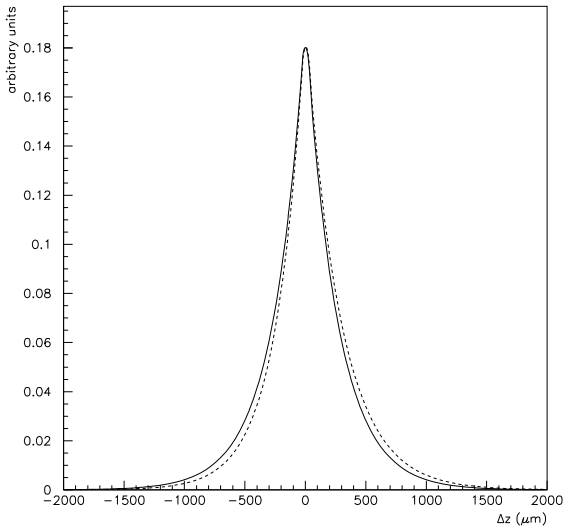

Figure 2: Theoretical Δz distribution for $\tau_B = 470$ μm and $(\beta\gamma)_{\Upsilon(4S)} = 0.556$. The solid curve is for a purely transverse $\Upsilon(4S)$ decay. The dashed line is for a decay with $(\beta\gamma)_{\rm rec} = 0.497$ and $(\beta\gamma)_{\rm tag} = 0.615$.

better than 100 μm for $p_T > 0.6$ GeV/c in the longitudinal (z) coordinate.

Particle identification facilitates the reconstruction of complex decay modes and of decays to J/ψ final states. Leptons and hadrons are identified using a combination of measurements from all the *BABAR* components, including the energy loss $\mathrm{d}E/\mathrm{d}x$ using a truncated mean of 40 samples (maximum) in the DCH and 5 samples in the SVT. Electrons and photons are identified in the barrel and the forward regions by the CsI electromagnetic calorimeter (EMC). Muons are identified in the instrumented flux return (IFR). In the central polar region, the Cerenkov ring imaging detector (DIRC) provides $> 3\sigma$ kaon identification for B decay products in the high momentum range where $\mathrm{d}E/\mathrm{d}x$ is no longer sensitive.

4 B reconstruction

The first step of this analysis is the reconstruction of B candidates. In section 4.1 we list the decay modes we reconstruct. The reconstruction procedure and the selection criteria we use are described in detail in other *BABAR* analysis documents [10, 11, 12]. In section 4.2 we just give a brief summary that focuses on a few aspects that are most relevant to the lifetime measurements. The final sample of reconstructed B candidates is described in section 4.3.

4.1 Decay modes reconstructed

The modes we reconstruct are listed in table 1. Here, and throughout this document, we use the convention that a particular candidate state also implies the charge conjugate state is included. In the same way, reference to a decay chain like

$$\overline{B}^0 \to D^{*+}\pi^-; D^{*+} \to D^0\pi^+; D^0 \to K^-\pi^+$$

also implies the charge conjugate decay chain is included.
The modes we reconstruct are clean two body decays to states that include either a charmed meson or a charmonium meson. The mesons including a c quark are reconstructed in their cleaner decay modes.
As B branching fractions tend to be small and the D or J/ψ branching fractions further reduce the yield for a given decay chain, we need to "add many drops in the bucket". We reconstruct 20 B^0 decay chains, including 2 that contain a J/ψ. In addition, we reconstruct 12 B^+ decay chains, including 4 that contain a J/ψ or a ψ' .

4.2 Reconstruction techniques

- PID for kaons
- mass cuts on intermediate states
- cut on Δm for D^*s, fit with beam spot contraint, blow up beam spot
- vertex χ^2 for a_1^+, K_S^0, D^0, D^+
- kinematic fits for π^0s
- Bremsstrahlung recovery for J/ψ
- variables for B reco:

$$\Delta E = E^*_{\rm meas} - E^*_{\rm beam}$$

$$m^2_{\rm ES} = (E^*_{\rm beam})^2 - \left(\sum_i \vec{p}^{\,*}_i\right)^2$$

- remove overlap, ΔE criterion
- background fighting
  - R2
  - thrust angle for less clean modes
- background fitting: Argus function [13]
- definition of purity (inside 2σ)

4.3 Sample composition

The substituted mass spectrum of our sample of B^0 candidates is shown in figure 3. A fit to the sum of the Argus background function plus a gaussian is superimposed. From this fit, we estimate the number of signal candidates as 2210 ± 58, with a purity of $\simeq 89\%$. The corresponding plot for the B^+ sample is shown in figure 4. The number of signal candidates is 2261 ± 53 with a purity of $\simeq 92\%$. The yields for each decay mode are listed in table 2.

We run the same reconstruction and selection procedure on all available generic Monte Carlo [14]. The substituted mass spectra, including a break-down of the different contributions to the background are shown in figures 5 and 6.

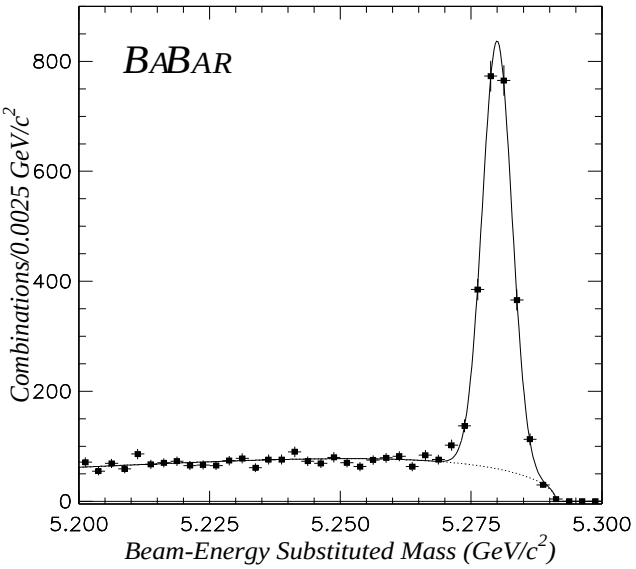

Figure 3: Substituted mass spectrum of the candidates in our B^0 sample.

5 Semileptonic B reconstruction

The details of the multistep data reduction procedure are given in another BAD document[12] from the B reco analysis working group. The characteristics of the reconstructed B_{rec} modes are detailed in section 5.3.

B^0		
	$D^{*+}\pi^-$, $D^{*+} \to D^0\pi^+$	$D^0 \to K^-\pi^+$
		$D^0 \to K^-\pi^+\pi^0$
		$D^0 \to K^0_S\pi^+\pi^-$
		$D^0 \to K^-\pi^+\pi^-\pi^+$
	$D^{*+}\rho^-$, $D^{*+} \to D^0\pi^+$	$D^0 \to K^-\pi^+$
	$\rho^- \to \pi^+\pi^0$	$D^0 \to K^-\pi^+\pi^0$
		$D^0 \to K^0_S\pi^+\pi^-$
		$D^0 \to K^-\pi^+\pi^-\pi^+$
	$D^{*+}a_1^-$, $D^{*+} \to D^0\pi^+$	$D^0 \to K^-\pi^+$
	$a_1^- \to \rho^0(\to \pi^+\pi^-)\pi^+$	$D^0 \to K^-\pi^+\pi^0$
		$D^0 \to K^0_S\pi^+\pi^-$
		$D^0 \to K^-\pi^+\pi^-\pi^+$
	$D^+\pi^-$	$D^+ \to K^-\pi^+\pi^+$
		$D^+ \to K^0_S\pi^+$
	$D^+\rho^-$	$D^+ \to K^-\pi^+\pi^+$
		$D^+ \to K^0_S\pi^+$
	$D^+a_1^-$	$D^+ \to K^-\pi^+\pi^+$
		$D^+ \to K^0_S\pi^+$
	$J/\psi K^{*0}$, $J/\psi \to \ell^+\ell^-$	$K^{*0} \to K^+\pi^-$
B^-		
	$D^0\pi^-$	$D^0 \to K^-\pi^+$
		$D^0 \to K^-\pi^+\pi^0$
		$D^0 \to K^0_S\pi^+\pi^-$
		$D^0 \to K^-\pi^+\pi^-\pi^+$
	$D^{*0}\pi^-$, $D^{*0} \to D^0\pi^0$	$D^0 \to K^-\pi^+$
		$D^0 \to K^-\pi^+\pi^0$
		$D^0 \to K^0_S\pi^+\pi^-$
		$D^0 \to K^-\pi^+\pi^-\pi^+$
	$J/\psi K^-$, $J/\psi \to \ell^+\ell^-$	
	$\psi' K^-$, $\psi' \to J/\psi\pi^+\pi^-$	
	$J/\psi \to \ell^+\ell^-$	

Table 1: Reconstructed decay chains.

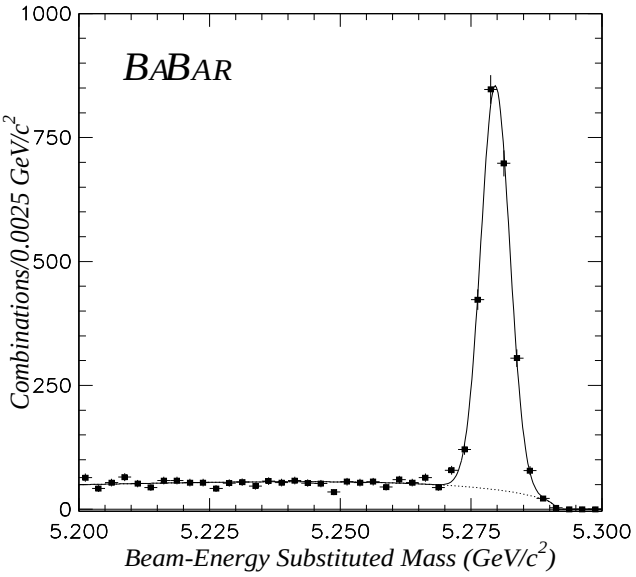

Figure 4: Substituted mass spectrum of the candidates in our B^+ sample.

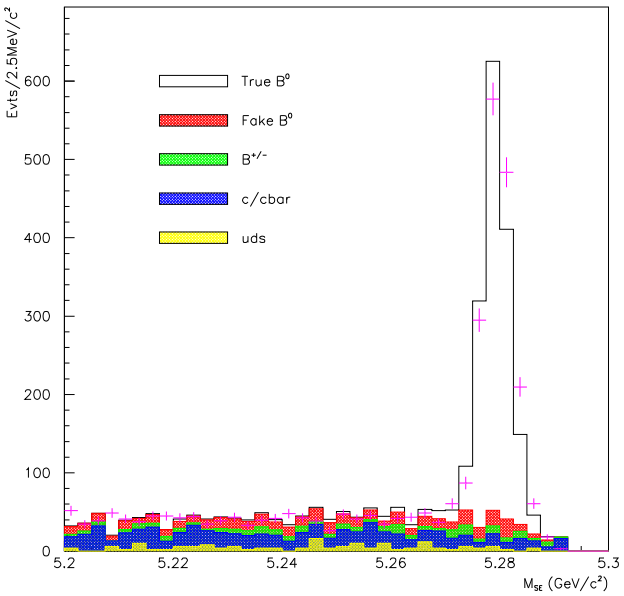

Figure 5: Substituted mass spectra of selected B^0 candidates on generic Monte Carlo.

Table 2: Two-body hadronic B^0 and B^- decay candidate yields and signal purities from the fit to the $m_{\rm SE}$ distribution.

Decay mode	Number of B candidates	S/(S+B) [%]
$B^0 \to D^{*-}\pi^+$	552±26	92
$B^0 \to D^{*-}\rho^+$	374±23	86
$B^0 \to D^{*-}a_1^+$	202±18	81
$B^0 \to D^-\pi^+$	537±25	92
$B^0 \to D^-\rho^+$	279±20	85
$B^0 \to D^-a_1^+$	194±18	77
$B^0 \to J/\psi K^{*0}$	167±15	91
$B^- \to D^0\pi^-$	1528±43	90
$B^- \to D^{*0}\pi^-$	446±25	90
$B^- \to J/\psi$,$\psi(2S)K^-$	294±17	99
Total B^0	2210±58	89
Total B^-	2261±53	92

5.1 Semileptonic chains

5.2 Data reduction

Summary of Breco BAD[12]

5.3 Sample composition and reconstruction efficiencies

the tables and figures of this section will be added after the sl B reco BAD are out

6 Vertex reconstruction and resolution function

The next step after the reconstruction of the B mesons and the event selection is the reconstruction of Δz, the observable we use as input to the lifetime fit. The event topology is sketched in figure 1 and the general strategy to measure the lifetime using Δz was discussed in section 2.
In measurements that use the decay length difference technique, it is more difficult to disentangle the effects of the lifetime and the detector resolution than in analyses where both the production and decay points of the particle in question are measured. In the latter analyses, the true proper decay times are distributed exponentially. In theory there should be no events at negative decay times. The negative part of the measured decay time distribution contains valuable information on the detector resolution. The width of the negative part tells us about the resolution, the positive part contains the combined effect of resolution and lifetime. For the decay length difference Δz, theory predicts a distribution that is symmetric

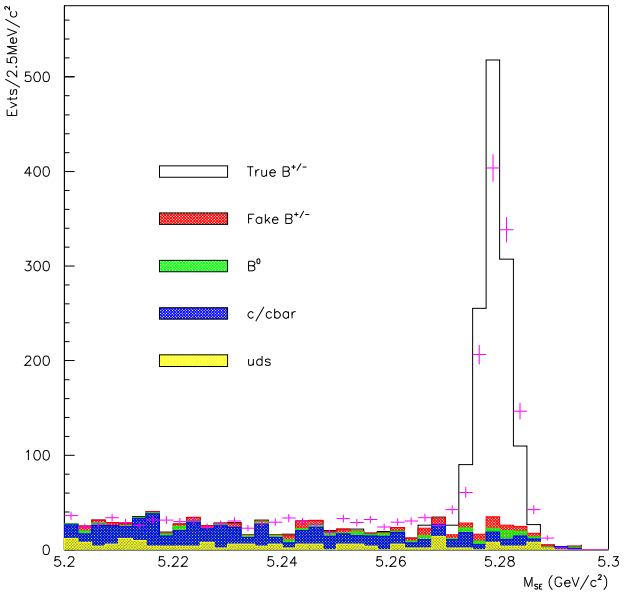

Figure 6: Substituted mass spectra of selected B^+ candidates on generic Monte Carlo.

around $\Delta z = 0$. The width of the distribution resulting from the convolution of the theoretical distribution with the resolution function carries information about the combined effect of the lifetime and the detector resolution. The information necessary to separate the two effects is in the form of the distribution. A detailed understanding of the resolution function is crucial for lifetime measurements using the decay length difference technique. We need to learn as much as possible from data about the resolution function.

In sections 6.1 and 6.3 we discuss the reconstruction of the vertices of the two B mesons in an event. The Δz resolution function is discussed in section 6.4. We isolate a zero lifetime control sample that we use to study the resolution function in data. This is discussed in section 6.5.

6.1 Vertex of the fully reconstructed B

We use the kinematic fitter GeoKin [15] to fit the vertex of the fully reconstructed B. GeoKin fits complete decay trees, proceeding leaf by leaf. For example, to fit the decay tree $B^- \to D^0\pi^-$, $D^0 \to K^-\pi^+$, first a fit of the $K^-\pi^+$ vertex is performed. Then the internal degrees of freedom of the D^0 candidate are frozen and a fit of the $D^0\pi^-$ vertex is performed. Additional constraints are applied in these fits. The masses of D^0 and J/ψ candidates are constrained to the PDG values. This constraint does not improve the vertex resolution, but it facilitates the candidate selection as it improves the ΔE resolution (see section 4). We constrain the vertex of D^{*+} candidates to be compatible with the beam spot. In the fits, we

use 40 μm as estimate of the size in y of the beam spot. This constraint improves the Δm resolution which also facilitates the candidate selection (see section 4). The decay vertices of short-living resonances (ρ^+, a_1^+, K^{*+}, K^{*0}, D^{*+} and J/ψ) are constrained to be identical to the decay vertex of the B.
The resolution on the vertex of the fully reconstructed B depends on the decay mode. Table 3 summarises values obtained from Monte Carlo for some typical decay modes. They range from roughly 45 μm to 65 μm for each coordinate. The corresponding pulls are around 1.1. The situation is slightly different for the y coordinate for modes involving a D^{*+} as we use the beam spot with a "blown up" estimate of its size. Our B selection criteria include the requirement that the kinematical fit of the decay tree has converged (section 4). The χ^2 probability distribution for Monte Carlo signal candidates in a characteristic mode is shown in figure 7. Figure 8 shows the same distribution for data (candidates in the signal region), all decay modes combined. We do not cut on the χ^2 probability.

Mode	$\sigma(x_{\rm rec})$	$\sigma(y_{\rm rec})$	$\sigma(z_{\rm rec})$	pull $x_{\rm rec}$	pull $y_{\rm rec}$	pull $z_{\rm rec}$
$\overline{B}^0 \to D^{*+}\pi^-$, $D^{*+} \to D^0\pi^+$, $D^0 \to K^-\pi^+$	45.3 ± 0.4	27.2 ± 0.2	45.0 ± 0.4	1.12 ± 0.01	0.93 ± 0.01	1.06 ± 0.01
$\overline{B}^0 \to D^{*+}\pi^-$, $D^{*+} \to D^0\pi^+$, $D^0 \to K^-\pi^+\pi^+\pi^-$	45.7 ± 1.2	26.2 ± 0.4	44.3 ± 0.7	1.09 ± 0.02	0.88 ± 0.01	1.03 ± 0.02
$\overline{B}^0 \to D^{*+}\rho^-$, $D^{*+} \to D^0\pi^+$, $D^0 \to K^-\pi^+$	61.3 ± 2.2	25.7 ± 0.7	65.7 ± 2.8	1.11 ± 0.03	0.79 ± 0.02	0.99 ± 0.02
$\overline{B}^0 \to D^{*+}a_1^-$, $D^{*+} \to D^0\pi^+$, $D^0 \to K^-\pi^+$	46.0 ± 1.8	25.4 ± 0.1	48.3 ± 1.7	1.13 ± 0.04	0.85 ± 0.03	1.07 ± 0.04
$\overline{B}^0 \to D^+\pi^-$, $D^+ \to K^-\pi^+\pi^+$	51.4 ± 0.8	53.1 ± 0.7	45.4 ± 0.6	1.10 ± 0.01	1.09 ± 0.01	1.02 ± 0.01
$B^- \to D^0\pi^-$, $D^0 \to K^-\pi^+$	53.0 ± 0.4	53.8 ± 0.5	48.6 ± 0.5	1.11 ± 0.01	1.13 ± 0.01	1.04 ± 0.01
$B^- \to J/\psi K^-$, $J/\psi \to e^+e^-/\mu^+\mu^-$	46.7 ± 0.5	46.6 ± 0.5	44.6 ± 0.5	1.15 ± 0.01	1.16 ± 0.01	1.07 ± 0.01

Table 3: Resolutions (μm) on the 3 coordinates of the $B_{\rm rec}$ vertex and the corresponding pulls for a few typical modes. A fit to two gaussians is used to estimate the resolutions and the weighed mean of the two widths is quoted.

6.2 Vertex of the reconstructed B in semileptonic modes

6.3 Opposite vertex

We use the VtxTagBtaSelFit algoritm [16, 17] to reconstruct the opposite vertex. This algorithm uses an inclusive technique to reconstruct the decay vertex of the opposite B. An

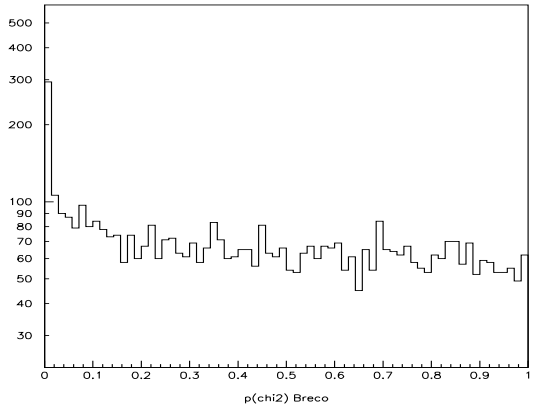

Figure 7: χ^2 probability for the kinematic fit of the $B_{\rm rec}$ decay tree for $B^0 \to D^-\pi^+$, $D^- \to K^+\pi^-\pi^-$ (signal Monte Carlo).

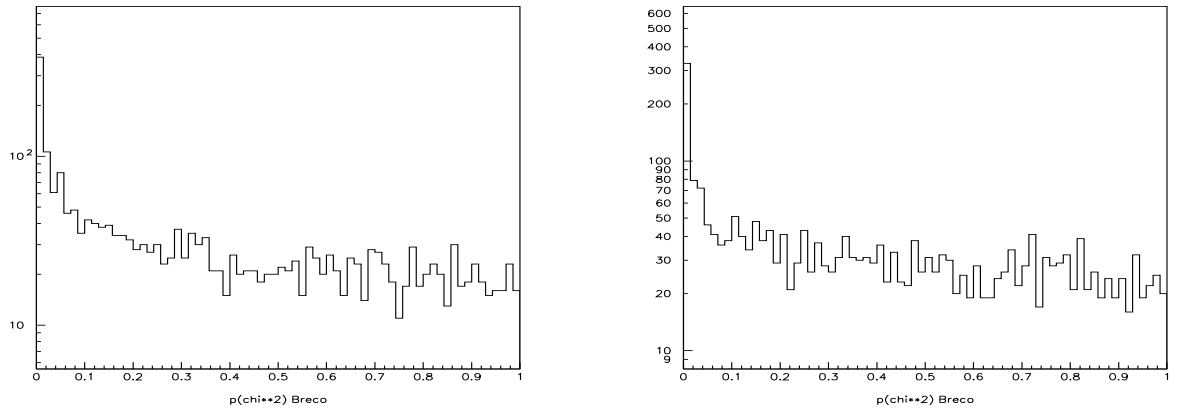

Figure 8: χ^2 probability for the kinematic fit of the $B_{\rm rec}$ decay tree for B candidates in the signal region (data). Left plot: all B^0 modes combined; right plot: all B^+ modes combined.

inclusive approach is needed to maintain a high efficiency. Complications can arise from the fact that we have to deal with secondary tracks that do not come directly from the opposite B, but from a long lived daughters of the opposite B.
Starting from those tracks in the event that have not been used to reconstruct the $B_{\rm rec}$, VtxTagBtaSelFit proceeds iteratively to select the tracks to be used to fit the opposite vertex. To reduce the bias due to tracks from long lived daughters, we reconstruct as many V^0s as possible and use these composite objects rather than their daughter tracks. Other secondary tracks are removed using a criterion based on their contribution to the χ^2 of the vertex fit. VtxTagBtaSelFit performs a fit of all input tracks and V^0s to a common vertex. In this fit, the fully reconstructed B is used as a "pseudo-track": from its reconstructed vertex and momentum, the beam spot position and size and from the $\Upsilon(4S)$ momentum we can get an estimate of the flight path of the opposite B (see figure 1). This procedure uses all information about the global event. All tracks and V^0s that contribute more than 5/ndof to the χ^2 of this global fit are rejected and the fit is repeated without them. This procedure is repeated until the list of input objects reaches stability. VtxTagBtaSelFit is highly efficient because the opposite vertex can be fit with just one direct track plus the "pseudo-track". For this particular analysis, however, we reject events in which only one track was used to fit the opposite vertex. The fraction of events with poorly reconstructed Δz is higher in the "one track" case then in the others (see section 6.4.3).

The residue $(z_{\rm opp})_{\rm generated} - (z_{\rm opp})_{\rm reconstructed}$ for the z position of the opposite vertex as well as the corresponding pull $\frac{(z_{\rm opp})_{\rm generated}-(z_{\rm opp})_{\rm reconstructed}}{\sigma(z_{\rm opp})}$ are shown in figure 9. The signal Monte Carlo events used to make these plots contain a fully reconstructed $B^- \to J/\psi K^-$. Fits to two gaussians are included in the plots. The resolution is $116 \pm 1 \mu$m and the residual bias is $26.3 \pm 1.0 \mu$m (weighed means over the two gaussians). A histogram of the number of tracks plus V^0s used to fit the opposite vertex is shown in figure 10.

The distribution of the error on Δz estimated event by event is shown in figures 11 and 12. A fit to the Crystal Ball lineshape function is superimposed. The χ^2 probability is plotted in figure 13. We require $\sigma(\Delta z) < 400$ μm and do not cut on $p(\chi^2)$. The reconstruction efficiency for the opposite vertex is xx % on Monte Carlo and xx % on data.

6.4 Delta z resolution function

The quality cuts applied after the Δz reconstruction are summarised in table 4. We now discuss some properties of the Δz resolution function.

The distribution of the Δz residue $\delta(\Delta z) = (\Delta z)_{\rm reconstructed} - (\Delta z)_{\rm generated}$ and the distribution of the corresponding pull $\frac{\delta(\Delta z)}{\sigma(\Delta z)}$ are shown in figure 9. Fits to the sum of two gaussians are superimposed on the histograms. From these fits we estimate the Δz resolution as 130 ± 1 μm and the bias as 24.5 ± 1.0 μm (weighed means over the two gaussians). The width of the pull distribution is 1.21 ± 0.01 and the mean is 0.29 ± 0.01.

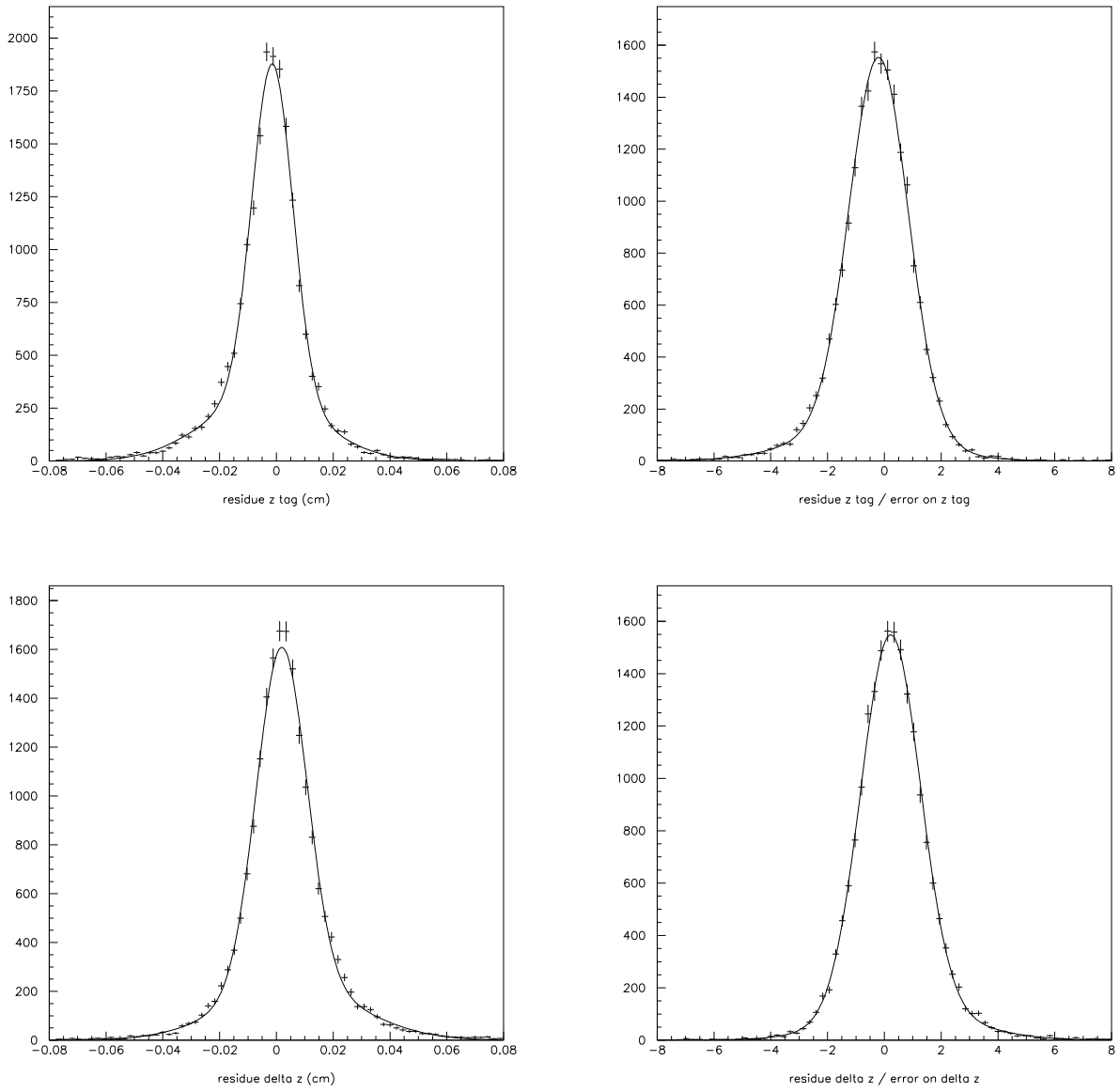

Figure 9: Top plots: residue (left) and pull (right) for the reconstructed z position of the opposite vertex. Bottom plots: residue (left) and pull (right) of the reconstructed Δz.

Figure 10: Number of tracks plus V^0s used to fit the opposite vertex. The points correspond to data, the histograms to Monte Carlo. Left: neutral Bs, right: charged Bs.

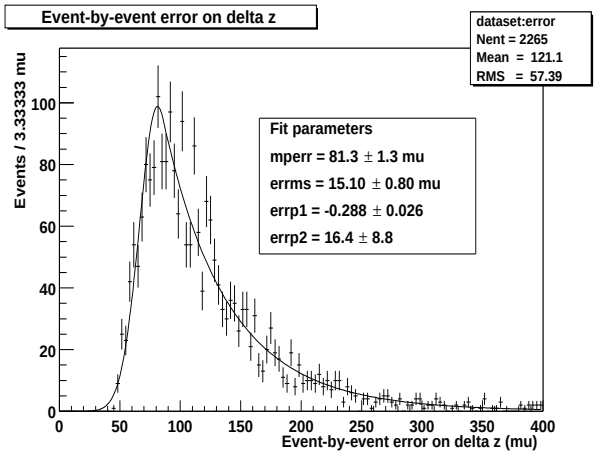

add MC plot

Figure 11: Event by event error on Δz for $B^0/\overline{B}^0$ events. Left: Monte Carlo, right data.

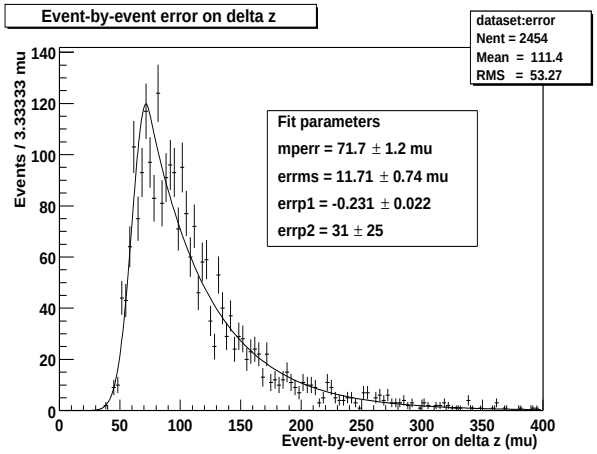

add MC plot

Figure 12: Event by event error on Δz for $B^{\pm}$ events. Left: Monte Carlo, right data.

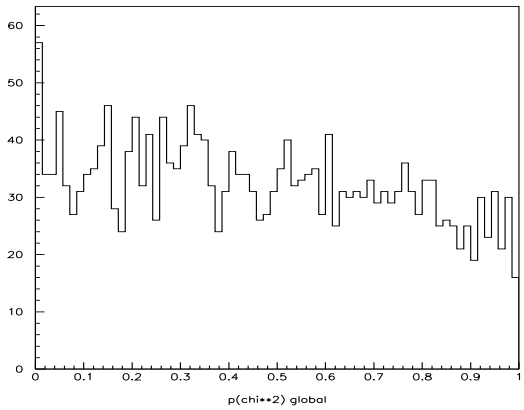

add MC plot

Figure 13: $p(\chi^2)$ for the global fit of $B^0/\overline{B}^0$ events. Left: Monte Carlo, right data.

$\sigma(\Delta z) < 400\ \mu$m
$\lvert\Delta z\rvert < 3000\ \mu$m
$n_{\rm track} \geq 2$

Table 4: Quality cuts applied after Δz reconstruction.

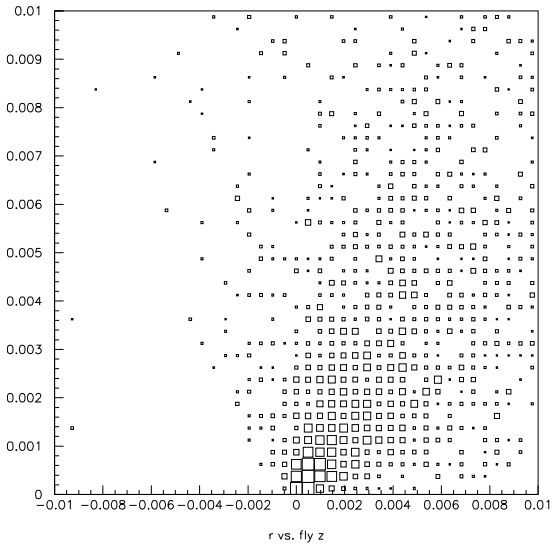

Figure 14: $r = \sqrt{x^2 + y^2}$ vs. z for the origin of tracks coming from the opposite B or its daughters. $r = 0$, $z = 0$ is defined to be the decay vertex of the opposite B.

6.4.1 Shape

From the fits shown in figure 9 and the fitted values quoted above we can see that the error on the opposite vertex dominates the error on Δz. The resolution on $z_{\rm rec}$ is typically 65 μm or better (table 3) and the resolution on $z_{\rm opp}$ is 116 μm. The reconstruction of $z_{\rm opp}$ is biased, resulting in a bias on Δz. This bias comes from secondary tracks used in the fit of the opposite vertex that have not been removed by the procedure described above. The generator level distribution of the origins of all tracks coming from the opposite B is plotted in figure 14. The relative position with respect to the decay vertex is plotted. Because of the boost, the daughters of the opposite B have the tendency to go into the forward direction. This results in the asymmetric distribution shown in figure 14. The effect of the secondary tracks is therefore not only to degrade the resolution on $z_{\rm opp}$, but also to bias the reconstruction. To illustrate this effect, we plot the Δz residue after a cut at generator level: we exclude all events that contain a D^+, D^0, D_s^+ or K_S^0 that flew more than 30 μm in z (figure 15). The Δz resolution becomes 118 μm and the bias is reduced to 7.5 μm.

The Δz resolutions and pulls for different $B_{\rm rec}$ decay modes are shown in figure 16. The

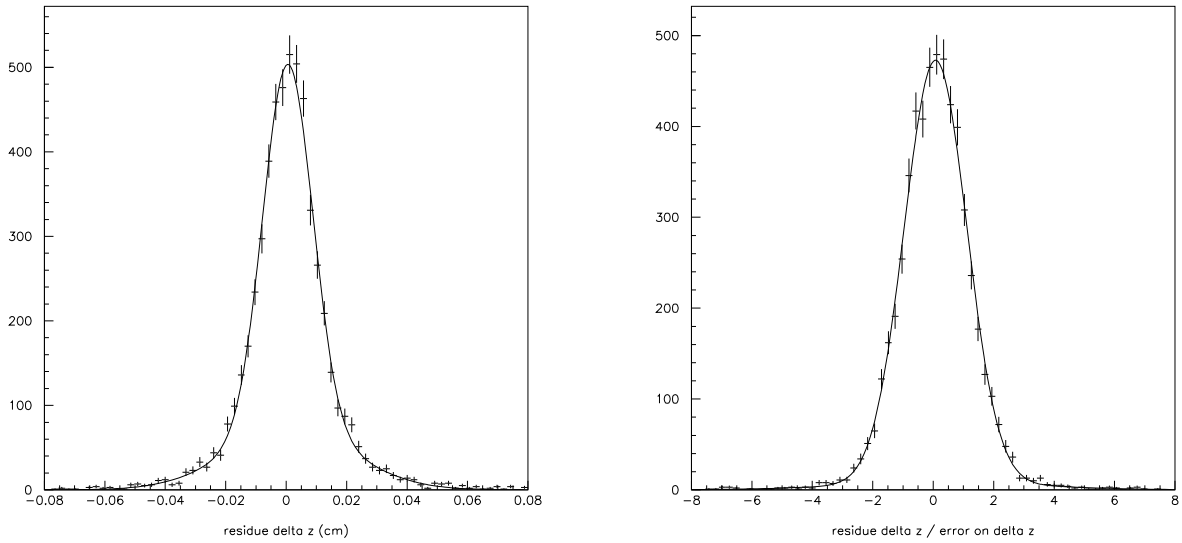

Figure 15: Δz residue (left) and pull (right) after cut at generator level: eliminate all events that contain a D^+, D^0, D_s^+ or K_S^0 that flew more than 30 μm in z.

distributions for different decay modes of one B species (B^0 or B^+) are compatible. The same is true for the values of parameters extracted from fits of two gaussians to these distributions. We expect this behaviour as the error on Δz is dominated by the error on the opposite vertex. We use only one single resolution function in the lifetime fit (see section 8) and not one per decay mode.
The distributions for charged and neutral Bs are also compatible. A discussion of this effect can be found in [20].

The Δz distributions measured in data and the Monte Carlo expectations are compared in figure 17.

6.4.2 Parameterisation

The Δz pull distribution (figure 9) is not gaussian. We try different parameterisations that we include into the likelihood function for the lifetime fit (section 8). Fits to the sum of two gaussians have already been shown above. This parameterisation uses five parameters: the fraction f of events in the narrow gaussian, the width s_1 and the bias b_1 of the narrow gaussian, and the width and bias of the wide gaussian (s_2,b_2). The fraction of events in the narrow gaussian is large ($\simeq 80\%$) and we also try the approximation of one single gaussian. This parameterisation uses two parameters.
Another parameterisation uses a gaussian with variable width and zero bias plus the same gaussian convoluted with a function that is zero for negative values and decreases exponentially for positive values. This parameterisation ("$G + G \otimes E$") uses three parameters: the fraction g of events in the central gaussian, the width s of the gaussian and the "lifetime" $\tau_{\rm r}$

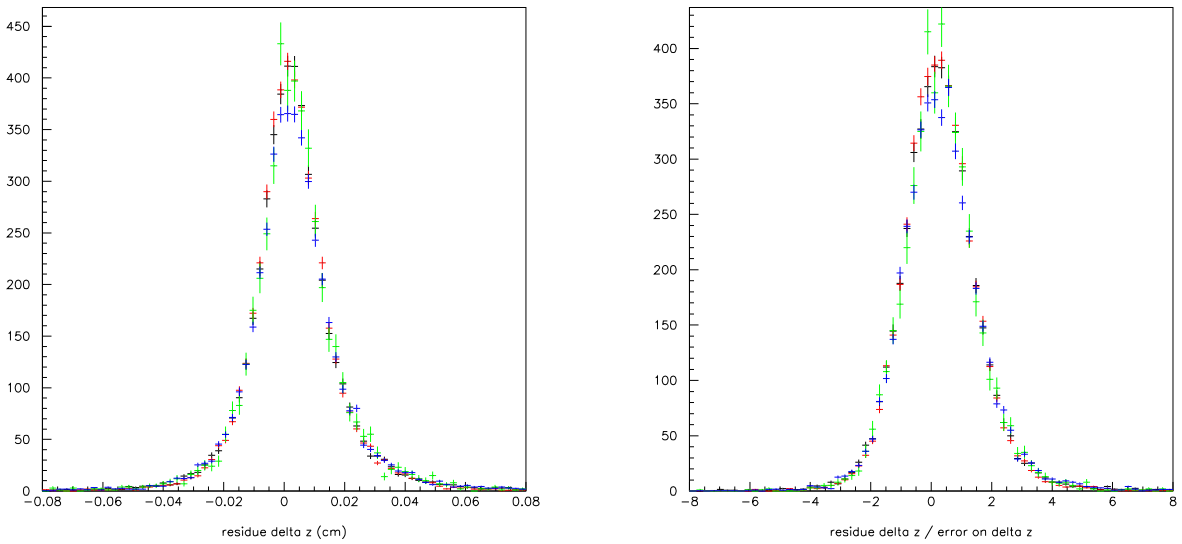

Figure 16: Δz residue (left) and pull (right) for different decay chains of the fully reconstructed B. Black: $B^- \to J/\psi K^-$, red: $B^- \to D^0\pi^-$, green: $\overline{B}^0 \to D^+\pi^-$ and blue: $\overline{B}^0 \to D^{*+}\pi^-$.

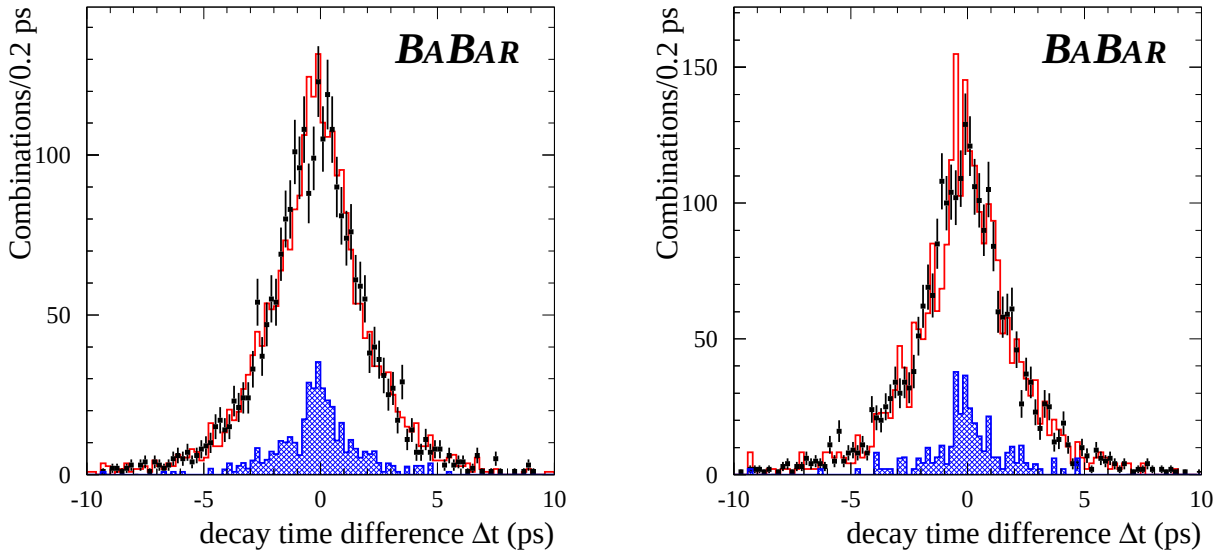

Figure 17: Comparison of Δt distributions for events in the signal region in the data (points) and generic Monte Carlo (red histogram; background contribution in blue). Left: neutral Bs, right: charged Bs. *For this plot: $\Delta z \to \Delta t$ and sign flipped. Equivalent as discussed in section 8. Eventually the whole BAD will be changed.*

	g	s	$\tau_{\rm r}$
$B^- \to J/\psi K^-$	0.678 ± 0.015	1.033 ± 0.008	0.956 ± 0.035
$B^- \to D^0\pi^-$	0.644 ± 0.020	1.008 ± 0.010	0.833 ± 0.037
$\overline{B}^0 \to D^+\pi^-$	0.637 ± 0.031	1.019 ± 0.017	0.914 ± 0.062
$\overline{B}^0 \to D^{*+}\pi^-$	0.666 ± 0.017	1.047 ± 0.010	1.024 ± 0.041

Table 5: Fits of the "$G+G\otimes E$" parameterisation to the diffent pull distributions in figure 16.

of the exponential. The results of fits of the "$G + G \otimes E$" parameterisation to the Δz pull obtained for different $B_{\rm rec}$ modes (right plot in figure 16) are summarised in table 5.
The results of fits using the three different parameterisations are plotted in figure 25. The fitted values for the three sets of parameters and the χ^2 values are given in table 8. The χ^2 values indicate that the two gaussians reproduce the pull distribution well. The χ^2 for "$G + G \otimes E$" is slightly worse and the χ^2 for one single gaussian is high, mainly because this parameterisation "has difficulties in reproducing the tail at positive pulls". Lifetime fits with these parameterisations are discussed in section 8.5.

6.4.3 Outliers

Plots and numbers given here include the "one track" case. Discuss this particular case.

The last plot in figure 9 shows the fit of two gaussians to the Δz pull for a sample of 20k reconstructed events. From the fit we would expect of the order of one event outside the region $-9 \leq \text{pull}(\Delta z) \leq 12$. This is roughly the region within 5 sigma from the centre of the wide gaussian. We observe 40 events outside, which corresponds roughly to 0.2 % of the events. These *outliers*, some of which are off by as much as 10 sigma, are not reproduced by our parameterisation of the resolution function. If not properly accounted for in the lifetime fit, this small fraction of events can introduce a bias on the fitted lifetime of the order of 1 % [20].
Figure 18 shows the error on Δz estimated event by event as a function of the residue. The events outside $-9 \leq \text{pull}(\Delta z) \leq 12$ are located between the residue axis and the two solid lines. The reconstructed Δz for these events is shown in figure 19.

6.5 Control sample

Most of the knowledge on the resolution function comes out of necessity from the SP3 Monte Carlo. Cross checking the resolution function on a real data sample is very much needed. The control sample that has been made comes from inclusive D* from continuum $c\bar{c}$ events where one D* is fully reconstructed and selected to lie in the backward direction ($cos\theta_{D^*} < 0$). The topology of the control events is sketched on Figure 20. Having set aside the tracks from the fully reconstructed D*, the remainder of the event (fragmentation tracks + charm prongs) can be subjected to the VtxTagBtaSelFit algorithm. One expects to find a no flight distribution smeared with a resolution function which mimics that for Δz in B$\bar{\rm B}$ events.

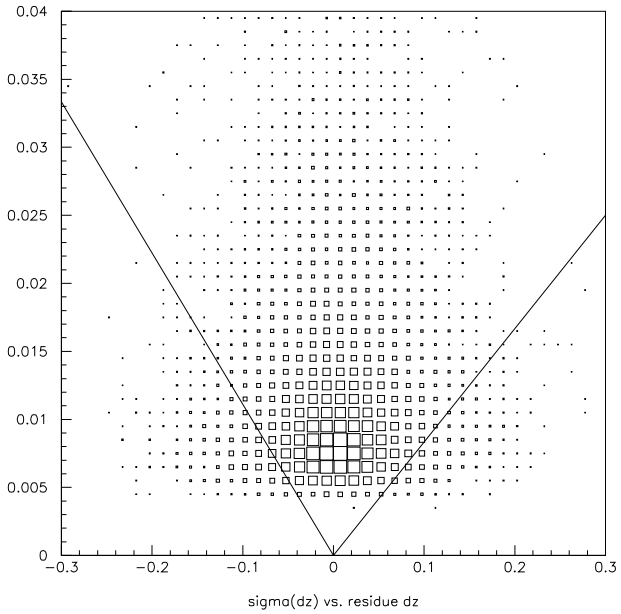

Figure 18: Error on Δz estimated event by event as a function of the residue. The events outside $-9 \leq \text{pull}(\Delta z) \leq 12$ (outliers) are located between the residue axis and the two solid lines.

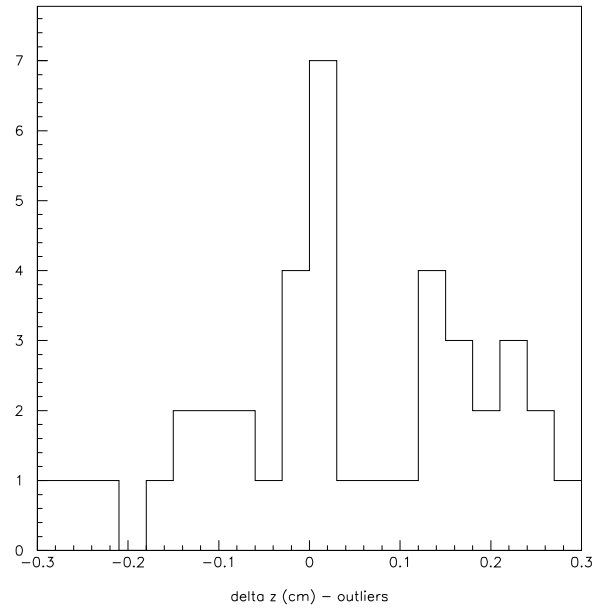

Figure 19: Δz for events outside $-9 \leq \text{pull}(\Delta z) \leq 12$ (outliers).

That was checked with SP3 Monte Carlo (Figure 21). The parameters of the 3 parameter fit on the real data Δz distribution (residue and pull assuming average is =0) from the control sample is shown on Figure 22. The agreement is fair given the low statistics of the samples on hand. The agreement between the pull distributions is the most satisfactory.

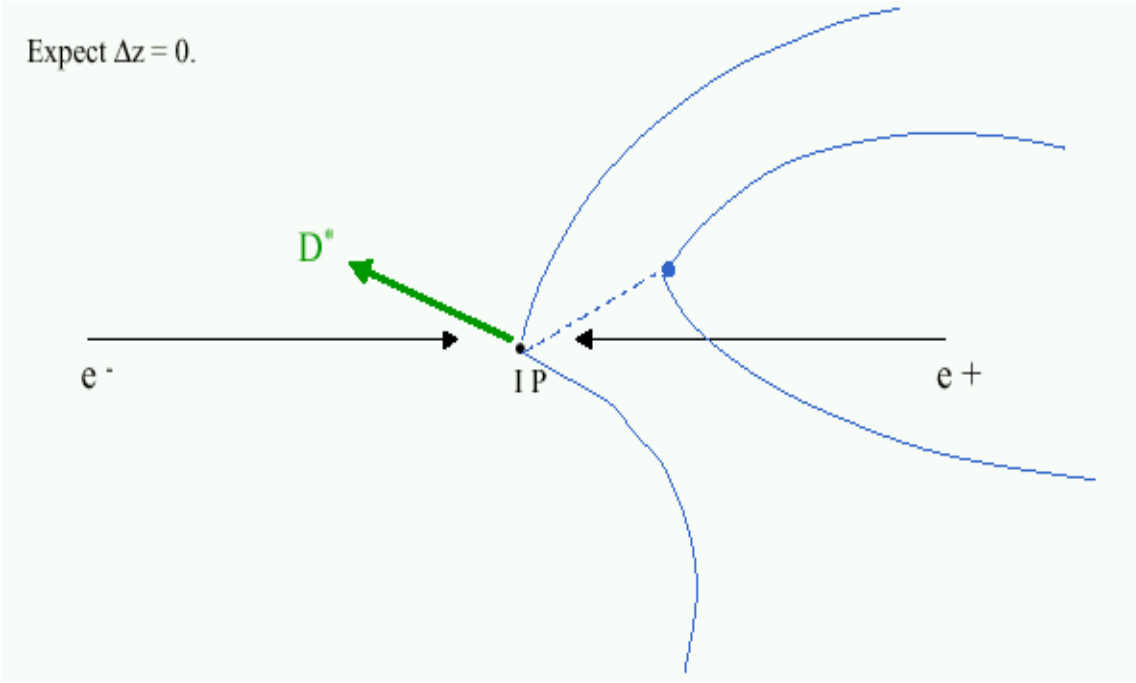

Figure 20: Topology of the events in the control sample.

6.6 Event displays

Some displays of typical events are in the works (WIRED).

Figure 21: (a) Distance between vertices for continuum events with a backward going fully reconstructed D* in SP3. 5 parameter fit results: bias-1=46$\pm$7 mum, σ-1= 124$\pm$6 μm, bias-2=262$\pm$ 148μm, σ-2=620$\pm$ 214 μm and fraction in the narrow gaussian = 76 $\pm$ 4%. (b) Corresponding pull distribution assuming average is zero. 3- parameter fit results: σ_p=0.92$\pm$0.04, τ_p=1.10 $\pm$ 0.17 and f$_p$=46 $\pm$ 8 %.

Figure 22: (a) Distance between vertices for continuum events with a backward going fully reconstructed D^* in the data (0.966 fb^{-1}). 5 parameter fit results: bias-1=36$\pm$8 mum, σ-1= 127$\pm$10 μm, bias-2=196$\pm$ 43μm, σ-2=317$\pm$ 31 μm and fraction in the narrow gaussian = 67 $\pm$ 7%. (b) Corresponding pull distribution assuming average is zero. 3- parameter fit results: σ_p=1.01$\pm$0.04, τ_p=1.34 $\pm$ 0.16 and f$_p$=47 $\pm$ 6 %.

7 Vertex reconstruction for semileptonic events

7.1 Vertex of the reconstructed B in a semileptonic mode

7.2 Opposite vertex

..... differences in the case of the sl events .....

7.3 Delta z resolution function

....

7.3.1 Outliers

..... differences in the case of a semileptonic B

7.4 Control sample

8 Lifetime fitting procedure

The measurement technique has been outlined in section 2. We reconstruct Δz and extract the B meson lifetimes from the Δz distribution of the selected events using an unbinned maximum likelihood fit. As discussed in section 2, in this fit we use an average value for $(\beta_z\gamma)_B$ of the B candidates. It is impossible to calculate the difference Δt of the proper decay times of the two B mesons in an event from Δz [19]. The exact calculation of Δt requires the knowledge of the common production point of the two B mesons. Using an average value for $(\beta_z\gamma)_B$ can be seen as making an approximate calculation of Δt. One could equivalently describe our fit in terms of this approximate Δt instead of Δz.

The present section describes the unbinned maximum likelihood fit. The Δz probability density function (PDF) for one event is a sum of three contributions. One to model the signal events in our data sample, one for the background and one for outliers (see section 6.4.3). The signal contribution is discussed in section 8.1, and the background in section 8.2. The modelling of outliers is discussed in section 8.3. Section 8.4 shows how we determine the signal probability for each event and how we use it to weigh the two contributions to obtain the full PDF and calculate the likelihood function. Section 8.5 summarises checks of the fitting procedure that we perform on Monte Carlo.

8.1 Signal modelling

The theoretical Δz distribution is plotted in figure 2. It is given by two exponential wings:

$$\phi(\Delta z) = \begin{cases} \frac{1}{\tau_B((\beta_z\gamma)_{\rm rec}+(\beta_z\gamma)_{\rm opp})} \cdot \exp\left(\frac{1}{\tau_B(\beta_z\gamma)_{\rm rec}} \cdot \Delta z\right) & \Delta z \leq 0 \\ \frac{1}{\tau_B((\beta_z\gamma)_{\rm rec}+(\beta_z\gamma)_{\rm opp})} \cdot \exp\left(-\frac{1}{\tau_B(\beta_z\gamma)_{\rm opp}} \cdot \Delta z\right) & \Delta z > 0 \ , \end{cases}$$

where $(\beta_z\gamma)_{\rm rec}$ describes the boost of the fully reconstructed B. As discussed in section 2, γ is calculated taking into account all three components of $\vec{\beta}$. $(\beta_z\gamma)_{\rm opp}$ is the corresponding quantity for the opposite B. In the fit we make the approximation $(\beta_z\gamma)_{\rm rec} = (\beta_z\gamma)_{\rm opp} = (\beta_z\gamma)_{\Upsilon(4S)}$, see section 2.

To obtain the PDF $\Phi(\Delta z)$ for the reconstructed Δz in a given event number i, we convolute the theoretical distribution $\phi(\Delta z)$ with the resolution function $\mathcal{R}(\delta(\Delta z), \sigma_i)$, where $\delta(\Delta z)$ denotes the residue and σ_i the error on Δz, estimated event by event.

$$\Phi(\Delta z) = \int_{-\infty}^{\infty} \phi\left(\overline{\Delta z}\right) \cdot \mathcal{R}\left(\Delta z - \overline{\Delta z}, \sigma_i\right) \ d\left(\overline{\Delta z}\right)$$

As discussed in section 6, the residue is not normally distibuted. We assume a certain functional form for $\mathcal{R}(\delta(\Delta z), \sigma_i)$ that contains additional parameters. These parameters will be let free in the fit for τ_B to avoid extracting their values from Monte Carlo. In section 6 we saw that we need to introduce enough free parameters to give our function the flexibility to reproduce the effect of measurement errors. The parameters in the resolution function tend to be strongly correlated to τ_B. Fitting simultaneously for correlated parameters increases the statistical error on all parameters. Quantitative examples of this effect can be found in section 8.5. A trade-off between statistical and systematic errors needs to be made. The choice of the parameterisation that minimises the total error depends on the size of the data sample.

We try different parameterisations of the resolution function. One of them uses two gaussians:

$$\begin{aligned} \mathcal{R}(\delta(\Delta z), \sigma_i; f, s_1, b_1, s_2, b_2) &= f \cdot \frac{1}{\sqrt{2\pi} \cdot \sigma_i s_1} \cdot \exp\left(-\frac{(\delta(\Delta z) - \sigma_i b_1)^2}{2\sigma_i^2 s_1^2}\right) \\ &\quad + (1-f) \cdot \frac{1}{\sqrt{2\pi} \cdot \sigma_i s_2} \cdot \exp\left(-\frac{(\delta(\Delta z) - \sigma_i b_2)^2}{2\sigma_i^2 s_2^2}\right) \end{aligned}$$

It contains five parameters: the fraction of events in the first gaussian (f), the width (s_1) and mean (b_1) of the first gaussian and the width (s_2) and mean (b_2) of the second gaussian. With this parameterisation we obtain

$$\begin{aligned} \Phi(\Delta z) &= f \cdot (c_1(s_1\sigma_i, b_1\sigma_i) + c_2(s_1\sigma_i, b_1\sigma_i)) \\ &\quad + (1-f) \cdot (c_1(s_2\sigma_i, b_2\sigma_i) + c_2(s_2\sigma_i, b_2\sigma_i)) \end{aligned}$$

with

$$
\begin{aligned}
c_1(s,b) &= \frac{1}{2\tau_B}\cdot\frac{1}{(\beta_z\gamma)_{\rm rec}+(\beta_z\gamma)_{\rm opp}} \\
&\quad\cdot\exp\left(\frac{s^2}{2\tau_B^2\cdot(\beta_z\gamma)_{\rm rec}^2}+\frac{1}{\tau_B(\beta_z\gamma)_{\rm rec}}\cdot(b-\Delta z)\right) \\
&\quad\cdot\,{\rm erfc}\left(\frac{s}{\sqrt{2}\tau_B(\beta_z\gamma)_{\rm rec}}+\frac{b-\Delta z}{\sqrt{2}s}\right)\ ,
\end{aligned}
$$

$$
\begin{aligned}
c_2(s,b) &= \frac{1}{2\tau_B}\cdot\frac{1}{(\beta_z\gamma)_{\rm rec}+(\beta_z\gamma)_{\rm opp}} \\
&\quad\cdot\exp\left(\frac{s^2}{2\tau_B^2\cdot(\beta_z\gamma)_{\rm opp}^2}+\frac{1}{\tau_B(\beta_z\gamma)_{\rm opp}}\cdot(\Delta z-b)\right) \\
&\quad\cdot\,{\rm erfc}\left(\frac{s}{\sqrt{2}\tau_B(\beta_z\gamma)_{\rm opp}}+\frac{\Delta z-b}{\sqrt{2}s}\right)
\end{aligned}
$$

and

$$
{\rm erfc}(x)=\frac{2}{\sqrt{\pi}}\int_x^\infty \exp(-t^2)\,dt\ .
$$

A different parameterisation uses one gaussian with variable width and zero bias plus the same gaussian convoluted with an exponential:

$$
\begin{aligned}
\mathcal{R}(\delta(\Delta z),\sigma_i;g,s,\tau_{\rm r}) &= g\cdot\frac{1}{\sqrt{2\pi}\cdot\sigma_i s}\cdot\exp\left(-\frac{(\delta(\Delta z))^2}{2\sigma_i^2 s^2}\right) \\
&+ (1-g)\cdot\frac{1}{2\cdot\sigma_i\tau_{\rm r}}\cdot\left[\exp\left(\frac{s^2}{2\tau_{\rm r}^2}-\frac{\delta(\Delta z)}{\sigma_i\tau_{\rm r}}\right)\cdot{\rm erfc}\left(\frac{s}{\sqrt{2}\tau_{\rm r}}-\frac{\delta(\Delta z)}{\sqrt{2}\cdot\sigma_i s}\right)\right]\ .
\end{aligned}
$$

It contains three parameters: the fraction g of events in the central gaussian, the width s of the gaussian and the "lifetime" $\tau_{\rm r}$ of the exponential. Using this parameterisation we obtain

$$
\begin{aligned}
\Phi(\Delta z) &= g\cdot(c_1(s\sigma_i,0)+c_2(s\sigma_i,0)) \\
&\quad +(1-g)\cdot(c_3(s\sigma_i,\tau_{\rm r}\sigma_i)+c_4(s\sigma_i,\tau_{\rm r}\sigma_i)+c_5(s\sigma_i,\tau_{\rm r}\sigma_i)+c_6(s\sigma_i,\tau_{\rm r}\sigma_i))
\end{aligned}
$$

with

$$
\begin{aligned}
c_3(w,\tau) &= \frac{1}{2}\cdot\frac{1}{\tau_B\cdot((\beta_z\gamma)_{\rm rec}+(\beta_z\gamma)_{\rm opp})+\tau\left(1+\frac{(\beta_z\gamma)_{\rm opp}}{(\beta_z\gamma)_{\rm rec}}\right)} \\
&\quad\cdot\exp\left(\frac{w^2}{2\tau_B^2(\beta_z\gamma)_{\rm rec}^2}-\frac{\Delta z}{\tau_B(\beta_z\gamma)_{\rm rec}}\right) \\
&\quad\cdot\,{\rm erfc}\left(\frac{w}{\sqrt{2}\tau_B(\beta_z\gamma)_{\rm rec}}-\frac{\Delta z}{\sqrt{2}w}\right)
\end{aligned}
$$

$$
\begin{aligned}
c_4(w,\tau) &= \frac{1}{2}\cdot\frac{1}{\tau_B\cdot((\beta_z\gamma)_{\rm rec}+(\beta_z\gamma)_{\rm opp})+\tau\left(1+\frac{(\beta_z\gamma)_{\rm opp}}{(\beta_z\gamma)_{\rm rec}}\right)} \\
&\quad\cdot\exp\left(\frac{w^2}{2\tau^2}+\frac{\Delta z}{\tau}\right) \\
&\quad\cdot{\rm erfc}\left(\frac{w}{\sqrt{2}\tau}+\frac{\Delta z}{\sqrt{2}w}\right)
\end{aligned}
$$

$$
\begin{aligned}
c_5(w,\tau) &= -\frac{1}{2}\cdot\frac{1}{\tau_B\cdot((\beta_z\gamma)_{\rm rec}+(\beta_z\gamma)_{\rm opp})-\tau\left(1+\frac{(\beta_z\gamma)_{\rm rec}}{(\beta_z\gamma)_{\rm opp}}\right)} \\
&\quad\cdot\exp\left(\frac{w^2}{2\tau^2}+\frac{\Delta z}{\tau}\right) \\
&\quad\cdot{\rm erfc}\left(\frac{w}{\sqrt{2}\tau}+\frac{\Delta z}{\sqrt{2}w}\right)
\end{aligned}
$$

$$
\begin{aligned}
c_6(w,\tau) &= \frac{1}{2}\cdot\frac{1}{\tau_B\cdot((\beta_z\gamma)_{\rm rec}+(\beta_z\gamma)_{\rm opp})-\tau\left(1+\frac{(\beta_z\gamma)_{\rm rec}}{(\beta_z\gamma)_{\rm opp}}\right)} \\
&\quad\cdot\exp\left(\frac{w^2}{2\tau_B^2(\beta_z\gamma)_{\rm opp}^2}+\frac{\Delta z}{\tau_B(\beta_z\gamma)_{\rm opp}}\right) \\
&\quad\cdot{\rm erfc}\left(\frac{w}{\sqrt{2}\tau_B(\beta_z\gamma)_{\rm opp}}+\frac{\Delta z}{\sqrt{2}w}\right)
\end{aligned}
$$

The sum of $c_5(w,\tau)$ and $c_6(w,\tau)$ is the result of a convolution of two exponentials with negative decay constants followed by a convolution with a gaussian. This sum, $c_5(w,\tau)+c_6(w,\tau)$, contains a mathematical pathology at $(\beta_z\gamma)_B\tau_B\simeq\tau$ that arises from the convolution of the two exponentials. The convolution of two functions of the form $\exp\left(-\frac{1}{\tau_1}\cdot x\right)$ and $\exp\left(-\frac{1}{\tau_2}\cdot x\right)$ results in a function of the form

$$
\frac{1}{\tau_1-\tau_2}\cdot\left[\exp\left(-\frac{1}{\tau_1}\cdot x\right)-\exp\left(-\frac{1}{\tau_2}\cdot x\right)\right]\ . \qquad (*)
$$

For $|(\beta_z\gamma)_B\tau_B-\tau|<10\ \ \mu$m we substitute

$$
\begin{aligned}
\tau_{\rm m} &= \frac{(\beta_z\gamma)_B\tau_B+\tau}{2} \\
\epsilon &= \frac{(\beta_z\gamma)_B\tau_B-\tau}{2}
\end{aligned}
$$

and develop the function of form (*) to zeroth order in $\frac{\epsilon}{\tau_{\rm m}}$. This results in a function of the form

$$
\frac{x}{\tau_{\rm m}^2}\cdot\exp\left(-x/\tau_{\rm m}\right)
$$

which can readily be convoluted with a gaussian. This procedure gives

$$\begin{aligned} c_5(w,\tau)+c_6(w,\tau) &\simeq c_7(w,\tau_{\rm m}) \\ &= \frac{1}{\sqrt{2\pi}\cdot\tau_{\rm m}^2 w}\cdot\exp\left(\frac{w^2}{2\tau_{\rm m}^2}-\frac{\Delta z}{\tau_{\rm m}}\right) \\ &\quad\cdot\left[w^2\cdot\exp\left(-\frac{1}{2w^2}\cdot\left(\frac{w^2}{\tau_{\rm m}}-\Delta z\right)^2\right)\right. \\ &\quad\left.-\sqrt{\frac{\pi}{2}}\cdot w\cdot\left(\frac{w^2}{\tau_{\rm m}}-\Delta z\right)\cdot{\rm erfc}\left(\frac{w}{\sqrt{2}\tau_{\rm m}}-\frac{\Delta z}{\sqrt{2}w}\right)\right]\ . \end{aligned}$$

8.2 Background modelling

We extract most of the information on the background properties from events in the substituted mass sideband. Figure 23 is a histogram of Δz for events with a $B^0/\overline{B}^0$ candidate in the substituted mass region between 5.2 GeV and 5.25 GeV. All modes are combined and the same cut on ΔE is applied as for the selection of signal events. The solid line represents the result of an unbinned maximum likelihood fit of the function

$$\begin{aligned} B(\Delta z;b_{\rm B},\sigma_{\rm B},f_{\rm pos},\tau_{\rm pos},f_{\rm neg},\tau_{\rm neg}) &= (1-f_{\rm pos}-f_{\rm neg})\cdot\frac{1}{\sqrt{2\pi}\sigma_{\rm B}}\cdot\exp\left(-\frac{(\Delta z-b_{\rm B})^2}{2\sigma_{\rm B}^2}\right) \\ &\quad+\begin{cases} f_{\rm neg}\cdot\frac{1}{\tau_{\rm neg}}\cdot\exp\left(\frac{\Delta z}{\tau_{\rm neg}}\right) & \Delta z\le 0 \\ f_{\rm pos}\cdot\frac{1}{\tau_{\rm pos}}\cdot\exp\left(\frac{-\Delta z}{\tau_{\rm pos}}\right) & \Delta z>0 \end{cases} \end{aligned}$$

(gaussian plus independent exponential tails towards positive Δz and negative Δz) to the Δz distribution of these sideband events.

The background is essentially combinatorial with contributions from both $b\overline{b}$ and continuum events; in particular $c\overline{c}$ events which are an abundant source of real D and D^* mesons. The background events from continuum tend to have small or zero "lifetimes", while background events from $b\overline{b}$ can have "lifetimes" of the same order of magnitude as the B lifetimes. Because of the machine boost, the Δz distribution of the background events is not necessarily symmetric around $\Delta z = 0$. We let the mean of the gausian free in the above fit on the sideband events and we do not force the positive and negative tails to be symmetric, i.e. have the same "lifetime" or fraction of events in them. This leads to a total of six free parameters in $B(\Delta z;b_{\rm B},\sigma_{\rm B},f_{\rm pos},\tau_{\rm pos},f_{\rm neg},\tau_{\rm neg})$: the mean $b_{\rm B}$ and width $\sigma_{\rm B}$ of the gaussian, the fraction of events in the positive tail $f_{\rm pos}$ and their "lifetime" $\tau_{\rm pos}$ plus the corresponding two parameters for the negative tail ($f_{\rm neg}$, $\tau_{\rm neg}$).

The results of the above fit are summarised in figure 23. The errors on the fit parameters are large, but our goal is not the precise determination of some parameter describing some background property. We only need a fitted function that reproduces the background Δz distribution. The mean of the gaussian is still consistent with zero within a large error.

The parameters describing the two different exponential tails are consistent; also within large errors. The "lifetimes" of the two exponentials are comparable to $< (\beta_z \gamma)_B > \cdot \tau_B$.

The corresponding histogram of Δz for events that contain a $B^{\pm}$ candidate in the substituted mass sideband region is show in figure 24. It shows the same features as the histogram for $B^0/\overline{B}^0$.

In our maximum likelihood fit for τ_B, we use the same parameterisation $B(\Delta z; b_{\rm B}, \sigma_{\rm B}, f_{\rm pos}, \tau_{\rm pos}, f_{\rm neg}, \tau_{\rm neg})$ as in the independent fits discussed above. All six parameters are free. In the fit for τ_B we do not explicitely distinguish between events in the signal region and sideband events. Instead, we assign a signal probability to each event depending on the substituted mass of the fully reconstructed B candidate it contains. The sideband events still dominate the determination of the parameters that describe the background, however.

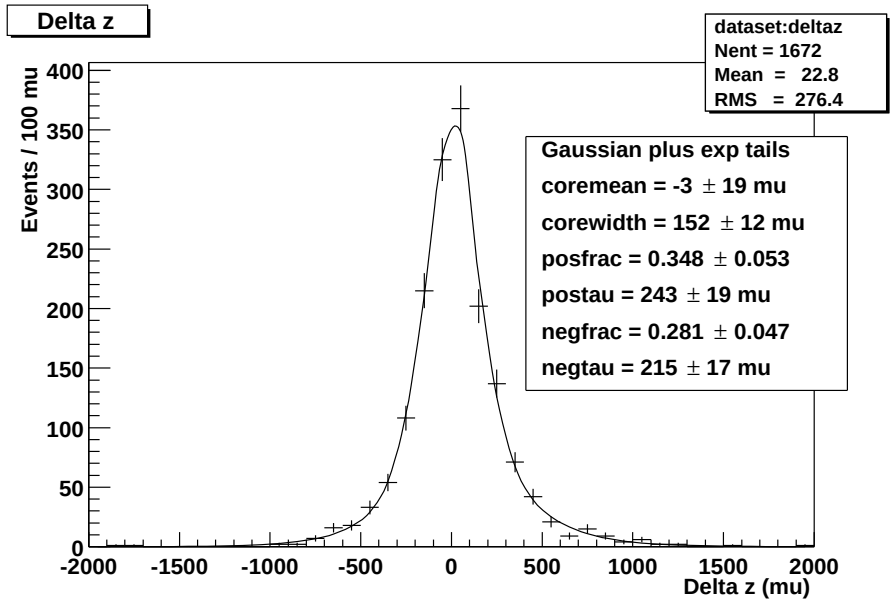

Figure 23: Δz distribution for events in the substituted mass sideband. All $B^0/\overline{B}^0$ modes combined. $\chi^2/\text{ndof} = 30.86/(40-6) = 0.91$ calculated from binned histogram and the result of the unbinned maximum likelihood fit.

8.3 Outliers

Our Δz reconstruction quality cuts include the requirement that $|\Delta z| < 3000$ μm (see table 4). Between -3000 μm and 3000 μm, we use a wide gaussian with a fixed width of $\sigma_{\rm out} = 2500$ μm and fixed mean of $b_{\rm out} = 1000$ μm to model the contribution of outliers to

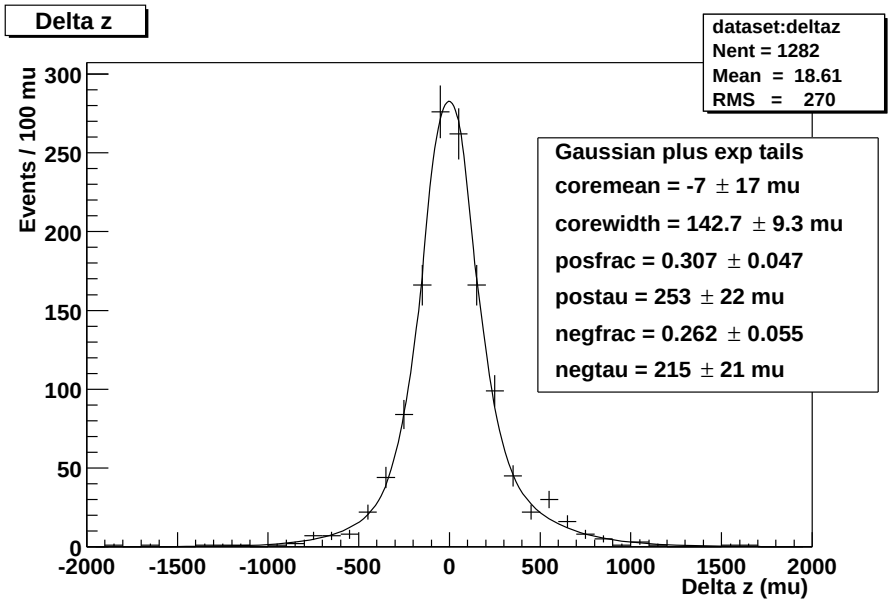

Figure 24: Δz distribution for events in the substituted mass sideband. All $B^{\pm}$ modes combined. $\chi^2/\mathrm{ndof} = 30.80/(40-6) = 0.91$ calculated from binned histogram and the result of the unbinned maximum likelihood fit.

the total Δz distribution (figure 19). We fit for the fraction of outliers f_{out}.

$$O(\Delta z; b_{\mathrm{out}}, \sigma_{\mathrm{out}}) = \frac{2}{2-\mathrm{erfc}\left(\frac{3000\ \mu\mathrm{m}-b_{\mathrm{out}}}{\sqrt{2}\sigma_{\mathrm{out}}}\right)-\mathrm{erfc}\left(\frac{b_{\mathrm{out}}+3000\ \mu\mathrm{m}}{\sqrt{2}\sigma_{\mathrm{out}}}\right)} \cdot \frac{1}{\sqrt{2\pi}\sigma_{\mathrm{out}}} \cdot \exp\left(-\frac{(\Delta z-b_{\mathrm{out}})^2}{2\sigma_{\mathrm{out}}^2}\right)$$

8.4 Likelihood function

We assign a signal probability $p_{\mathrm{sig},i}$ to each event i. It is based on the substituted mass of the fully reconstructed B in the event and is derived from an independent fit of the Argus background function plus a gaussian to the substituted mass distribution of the fully reconstructed B candidates in our sample. One single fit to the substituted mass distribution of all B candidates of one species in our sample is performed, combining all modes. The purities for different modes that we reconstruct are different. This additional information could be exploited by taking into account the decay mode of the B candidate when calculating $p_{\mathrm{sig},i}$. In this case, fits to the substituted mass distributions for each mode need to be used. The background also needs to be modelled for each mode separately. This is a refinement that can be added easily once more statistics is available.

The negative log-likelihood function that we minimise in the fit is

$$\mathcal{L} = -\sum_i \log\{[\quad p_{\mathrm{sig},i} \cdot \Phi\left((\Delta z)_i, \sigma_i; \{f, s_1, b_1, s_2, b_2\} \text{ or } \{g, s, \tau_\mathrm{r}\}\right) + (1 - p_{\mathrm{sig},i} - f_\mathrm{out}) \cdot B((\Delta z)_i; b_\mathrm{B}, \sigma_\mathrm{B}, f_\mathrm{pos}, \tau_\mathrm{pos}, f_\mathrm{neg}, \tau_\mathrm{neg}) + f_\mathrm{out} \cdot O((\Delta z)_i; b_\mathrm{out}, \sigma_\mathrm{out})] \cdot \rho(\sigma_i)\} \ ,$$

where $\rho(\sigma_i)$ is the distribution of the event by event errors on Δz. We use a fit of the Crystall Ball line shape function [18] to the distribution obtained for our data sample, see figure xxx in section 6.

The measured variables for a given event i are $(\Delta z)_i$, the associated error σ_i and the signal probability $p_{\mathrm{sig},i}$. Both these input variables and the free parameters in the fit are summarised in table 6.

At the present level of statistical precision, the resolution functions for neutral and charged Bs are compatible (section 6.4.1). We perform a combined fit to the Δz distributions of our two samples. The two Δz distributions are not combined. They are fitted simultaneously, but separately and with different sets of parameters to describe the background, the lifetime, etc. The only link between the two fits comes from the use of the same values for the parameters that describe the resolution function. Mathematically speaking, we minimise the sum of two terms of the form of $\mathcal{L}$, which have a subset of parameters in common.

8.5 Tests with Monte Carlo

We implement the unbinned maximum likelihood fit described above using the $\mathrm{t\bar{t}}$ RooFitTools package [21]. To test the implementation we generate sets of toy Monte Carlo samples for both neutral and charged Bs with parameter values close to the ones we get from full Monte Carlo. We then use our fitting program to extract the lifetime.
We generate 500 samples for each species and each parameterisation of the resolution function. The input lifetime τ_gen and the average fitted lifetime τ_fit for the different sets of samples are listed in table 7. We observe a hint of a small negative bias for the fitted lifetimes of both species. We attribute it to numerical problems. We fit the lifetime pull distributions $(\frac{\tau_\mathrm{fit}-\tau_\mathrm{gen}}{\sigma_\mathrm{fit}})$ to a single gaussian to check the estimated uncertainty on the fitted lifetime. From the width of the pull distributions we conclude that the lifetime uncertainties are calculated correctly (see table 7).

We use a sample of 5k fully reconstructed signal Monte Carlo events ($\mathrm{t\bar{t}}$ BBsim full simulation) for the decay chain $B^0 \to D^-\pi^+$, $D^- \to K^+\pi^-\pi^-$ to compare different parameterisations of the resolution function. Figure 25 shows fits of three different functions to the Δz pull distribution: a single gaussian and the two parameterisations described above. The fitted values for the three sets of parameters are summarised in table 8.

We use our fitting procedure to extract the lifetime from these events, using a signal probability of one for all events. We try both parameterisations of the resolution function

Input variable		Description
$(\Delta z)_i$		decay length difference
σ_i		uncertainty on decay length difference
$p_{\mathrm{sig},i}$		signal probability
Parameter		**Description**
τ_B		signal lifetime
Resolution function:		
either	f	fraction of events in central gaussian
	s_1	width of central gaussian
	b_1	mean of central gaussian
	s_2	width of wide gaussian
	b_2	mean of wide gaussian
or	g	fraction of events in central gaussian
	s	width of central gaussian
	τ_{r}	"lifetime" of the exponential that models the effect of the charm flight
Background:		
	b_{B}	mean of the gaussian
	σ_{B}	width of the gaussian
	f_{pos}	fraction of events in the tail at positive Δz
	τ_{pos}	"lifetime" of the exponential that models the tail at positive Δz
	f_{neg}	fraction of events in the tail at negative Δz
	τ_{neg}	"lifetime" of the exponential that models the tail at negative Δz

Table 6: Description of input variables for each event and fit parameters used in the unbinned maximum likelihood lifetime fit.

Resolution function	B species	τ_{gen} (μm)	τ_{fit} (μm)	τ pull mean	τ pull width
$G + G \otimes E$	$B^0/\overline{B}^0$	470.0	468.9 $\pm$ 0.7	-0.087 $\pm$ 0.064	1.038 $\pm$ 0.057
	$B^{\pm}$	495.0	493.2 $\pm$ 0.8	-0.126 $\pm$ 0.050	1.103 $\pm$ 0.039
$G_1 + G_2$	$B^0/\overline{B}^0$	470.0			
	$B^{\pm}$	495.0			

Table 7: Results of the lifetime fits to toy Monte Carlo samples.

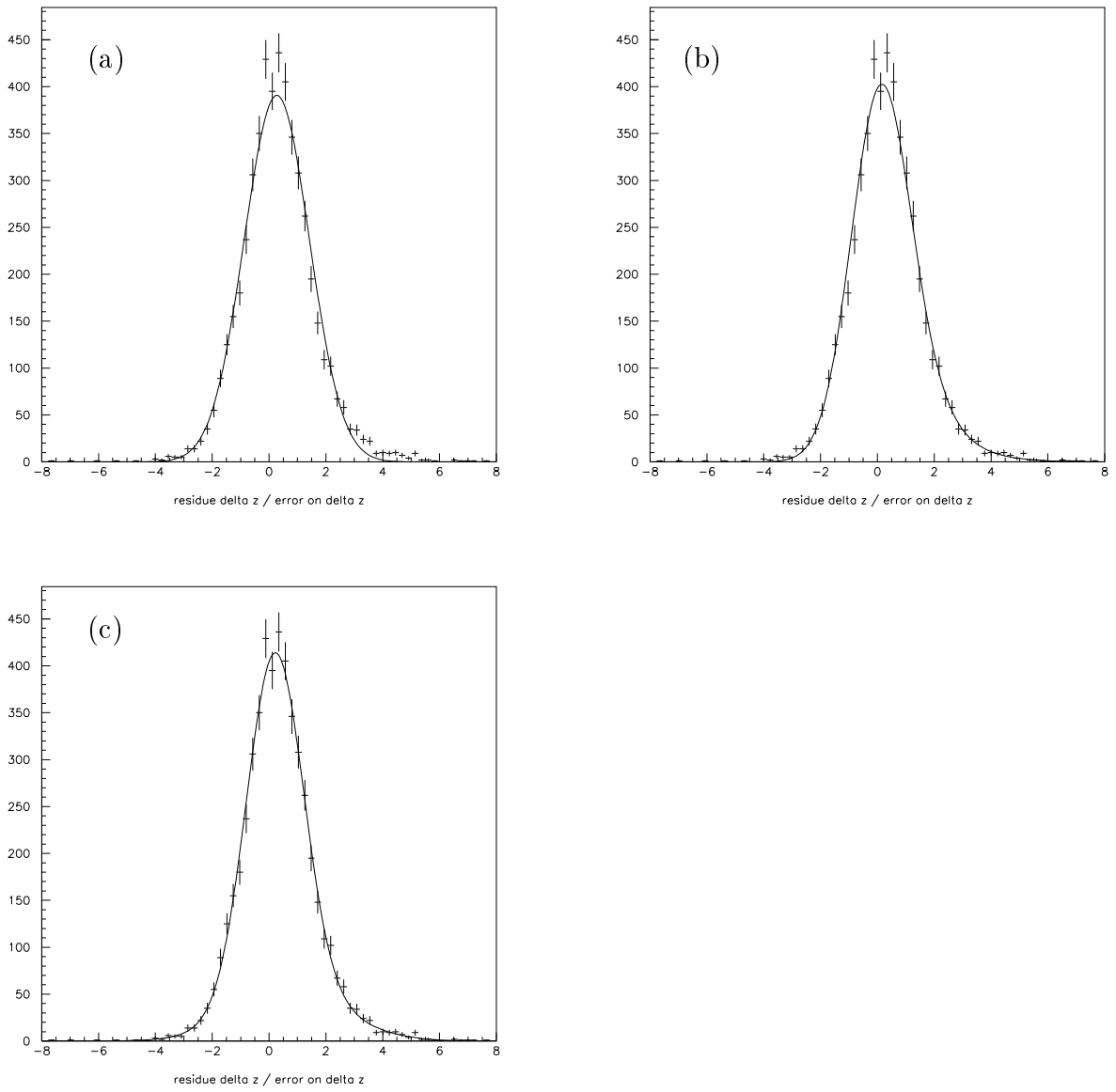

Figure 25: Fits of three different functions to the Δz pull: (a) a single gaussian, (b) a gaussian centred at zero plus the same gaussian convoluted with an exponential, (c) two gaussians. The fitted values for the parameters are summarised in table 8.

Single gaussian ("G")	mean = 0.273 ± 0.017	
	width = 1.148 ± 0.015	χ^2/ndof = 135.3/51
Gaussian centred at zero plus	g = 0.643 ± 0.029	
the same gaussian convoluted with an	s = 1.012 ± 0.0164	
exponential ("G+G⊗E")	τ_r = 0.936 ± 0.062	χ^2/ndof = 62.8/50
Two gaussians ("G+G")	f = 0.808 ± 0.047	
	s_1 = 0.998 ± 0.032	
	b_1 = 0.204 ± 0.025	
	s_2 = 1.931 ± 0.143	
	b_2 = 0.819 ± 0.139	χ^2/ndof = 40.0/48

Table 8: Values of the parameters for the different fits plotted in figure 25.

described in section 8.1. For the fit of two gaussians to the pull distribution, the fraction of events in the wide gaussian is small (see table 8). We also try fixing this fraction at zero, i.e. using one single gaussian. For all three different lifetime fits we only take into account events that satisfy $-5 \leq \text{pull}(\Delta z) \leq 8$. The effect of outliers is discussed elsewhere (section 12.6). The results of the lifetime fits are given in table 9. We repeat the three fits fixing the parameters that describe the resolution function at the values obtained using Monte Carlo truth and listed in table 8. The results of these fits are also listed in table 9.
We first discuss the results obtained with fixed resolution function. In this case the statistical errors for the three different parameterisations are roughly the same. The χ^2 values in table 8 indicate that the two gaussians give the most precise reproduction of the resolution function. The other two parameterisations underestimate the width of the pull distribution, either on the positive side or on the negative side. The effect is more pronounced for the parameterisation using one single gaussian. Consequently, these two parameterisations systematically lead to higher values for the lifetime than the fit with two gaussians. For "G+G⊗E" the difference is 1.5 μm (0.3 %), for "G" the difference is 6.3 μm (1.4 %).
When we free all parameters, the statistical uncertainty on the lifetime increases as we simultaneously fit for correlated parameters. The loss of precision is smallest for "G+G⊗E" and largest for "G+G".
"G" gives neither better statistical nor better systematic errors than "G+G⊗E". We do not use "G" in this analysis. "G+G" gives the smallest systematic error, but we expect "G+G⊗E" to give the smallest total uncertainty for the relatively low statistics currently available.

9 Lifetime fitting procedure (semileptonic modes)

	All parameters free	Fixed resolution function
Single gaussian ("G")	$\boldsymbol{\tau_B = 482.0 \pm 9.5\ \mu m}$ mean $= 0.28 \pm 0.04$ width $= 1.16 \pm 0.09$	$\boldsymbol{\tau_B = 482.8 \pm 7.4\ \mu m}$
Gaussian centred at zero plus the same gaussian convoluted with an exponential ("G+G⊗E")	$\boldsymbol{\tau_B = 478.8 \pm 8.2\ \mu m}$ $g = 0.66 \pm 0.09$ $s = 1.03 \pm 0.10$ $\tau_r = 0.87 \pm 0.20$	$\boldsymbol{\tau_B = 478.0 \pm 7.6\ \mu m}$
Two gaussians ("G+G")	$\boldsymbol{\tau_B = 469.8 \pm 11.38\ \mu m}$ $f = 0.83 \pm 0.14$ $s_1 = 0.96 \pm 0.17$ $b_1 = 0.26 \pm 0.08$ $s_2 = 2.56 \pm 0.75$ $b_2 = 0.38 \pm 0.48$	$\boldsymbol{\tau_B = 476.5 \pm 7.4\ \mu m}$

Table 9: Results of lifetime fits on full Monte Carlo using three different parameterisations of the resolution function. The generated lifetime is 468 μm.

10 Results of the fit to the data

Parameters:
1-5: mass spectrum B0
6-8: outliers B0
(fraction in per mil)
9-13: mass spectrum B+
14-16: outliers B+
(fraction in per mil)
17: lifetime B0
18-20: resolution function
21-24: error spectrum B0
25-30: background B0
31: lifetime B+
32-35: error spectrum B+
37-41: background B+

```
MIGRAD MINIMIZATION HAS CONVERGED.
MIGRAD WILL VERIFY CONVERGENCE AND ERROR MATRIX.
COVARIANCE MATRIX CALCULATED SUCCESSFULLY
FCN=95037.4 FROM MIGRAD    STATUS=CONVERGED     871 CALLS         872 TOTAL
                     EDM=0.014851    STRATEGY= 2      ERROR MATRIX ACCURATE
 EXT PARAMETER                                   STEP         FIRST
 NO.   NAME      VALUE            ERROR          SIZE      DERIVATIVE
  1  endptB0      5.29000e+00   constant
  2  cB0         -3.44000e+01   constant
  3  bmassB0      5.27992e+00   constant
  4  bresnB0      2.77400e-03   constant
  5  fB0          4.85300e-01   constant
  6  outFracB0    2.42968e+00   2.02331e+00   3.83458e-01   4.27950e-03
  7  outWidthB0   2.50000e+03   constant
```

```
  8  outMeanB0     0.00000e+00   constant
  9  endptCh       5.29000e+00   constant
 10  cCh          -3.17000e+01   constant
 11  bmassCh       5.27961e+00   constant
 12  bresnCh       2.65500e-03   constant
 13  fCh           5.86700e-01   constant
 14  outFracCh     5.41532e+00   2.41452e+00   4.78005e-01   1.64777e-04
 15  outWidthCh    2.50000e+03   constant
 16  outMeanCh     0.00000e+00   constant
 17  tauB0         4.53285e+02   1.56148e+01   2.70452e+00   2.78867e-03
 18  sigma         1.39260e+00   9.87260e-02   1.57232e-02  -3.43843e-01
 19  tau           6.32963e-01   1.90749e-01   2.30046e-02  -4.17284e-02
 20  frac          5.81247e-01   1.46551e-01   1.67997e-02   3.60181e-01
 21  mperrB0       8.13000e+01   constant
 22  errmsB0       1.51000e+01   constant
 23  errp1B0      -2.88000e-01   constant
 24  errp2B0       1.64000e+01   constant
 25  coremeanB0    7.42061e+00   1.77400e+01   2.18725e+00   4.63107e-04
 26  corewidthB0    1.57727e+02   1.05713e+01   1.88353e+00   7.29687e-04
 27  posfracB0     3.36887e-01   5.69347e-02   4.38786e-03   1.29615e-01
 28  postauB0      2.43268e+02   2.20186e+01   2.36255e+00   9.40266e-05
 29  negfracB0     2.84261e-01   5.21596e-02   4.15011e-03   8.19075e-02
 30  negtauB0      2.12113e+02   1.95193e+01   2.29640e+00   2.89542e-04
 31  tauCh         4.82199e+02   1.45700e+01   2.56697e+00  -6.87389e-03
 32  mperrCh       7.17000e+01   constant
 33  errmsCh       1.17100e+01   constant
 34  errp1Ch      -2.31000e-01   constant
 35  errp2Ch       3.10000e+01   constant
 36  coremeanCh   -3.01658e+00   1.82100e+01   2.25490e+00   4.19185e-04
 37  corewidthCh    1.43332e+02   9.73141e+00   1.80830e+00   8.50374e-04
 38  posfracCh     3.29935e-01   5.13827e-02   4.69476e-03   1.11723e-01
 39  postauCh      2.44675e+02   2.27059e+01   2.74679e+00   5.31431e-05
 40  negfracCh     2.89687e-01   5.64696e-02   4.98197e-03   3.84604e-02
 41  negtauCh      1.91814e+02   1.86451e+01   2.39605e+00   2.44862e-04
                            ERR DEF= 0.5
EXTERNAL ERROR MATRIX.    NDIM=  41    NPAR= 19    ERR DEF=0.5
ELEMENTS ABOVE DIAGONAL ARE NOT PRINTED.
 4.094e+00
-2.739e-03  5.830e+00
-7.033e+00 -3.667e-01  2.438e+02
 1.340e-02  5.068e-03 -8.007e-01  9.747e-03
-2.316e-02  1.773e-02  5.301e-01 -5.410e-03  3.639e-02
-1.288e-02  1.181e-02  3.389e-01 -2.471e-03  2.309e-02  2.148e-02
-3.000e-01  1.870e-02  1.551e+00  4.709e-04  3.152e-02  4.840e-02  3.147e+02
 7.204e-01 -1.213e-02  2.625e+00 -2.339e-02  1.345e-02  1.273e-02  1.010e+01  1.118e+02
 3.191e-02 -6.925e-05 -3.220e-02  4.571e-06 -1.145e-04 -4.039e-06 -3.125e-01 -1.545e-01  3.242e-03
-1.565e+01  4.054e-03  7.815e+00 -7.205e-03  1.723e-02  1.914e-02  5.315e+01  9.088e+00 -1.028e+00  4.848e+02
 2.860e-02 -6.122e-05 -2.806e-02 -4.091e-06 -9.335e-05 -5.486e-05  2.663e-01 -1.322e-01  2.164e-03 -8.174e-01  2.721e-03
-1.379e+01  4.905e-03  5.909e+00 -1.682e-02  2.927e-02 -1.772e-02 -3.758e+01 -3.768e+00 -7.598e-01  2.932e+02 -7.895e-01
-1.379e+01  4.905e-03  5.909e+00 -1.682e-02  2.927e-02 -1.772e-02 -3.758e+01 -3.768e+00 -7.598e-01  2.932e+02 -7.895e-01  3.810e+02
-3.696e-01 -7.848e+00  4.354e+01 -5.432e-01 -4.809e-01 -2.939e-01 -4.503e-01  1.368e+00  3.174e-03  1.916e-01  2.542e-03
-3.696e-01 -7.848e+00  4.354e+01 -5.432e-01 -4.809e-01 -2.939e-01 -4.503e-01  1.368e+00  3.174e-03  1.916e-01  2.542e-03  6.730e-02  2.123e+02
 1.107e-02 -3.732e-01 -8.090e-01  1.337e-02  1.282e-02  2.971e-02  1.025e-01 -1.255e-02  1.457e-04  2.393e-02 -4.490e-05
 1.107e-02 -3.732e-01 -8.090e-01  1.337e-02  1.282e-02  2.971e-02  1.025e-01 -1.255e-02  1.457e-04  2.393e-02 -4.490e-05 -1.146e-01 -4.565e-02  3.316e+02
-2.018e-02  8.072e-01  1.264e+00 -1.525e-02  7.076e-03  4.168e-03  2.933e-03  3.774e-02  1.004e-05  1.228e-02  1.151e-05
-2.018e-02  8.072e-01  1.264e+00 -1.525e-02  7.076e-03  4.168e-03  2.933e-03  3.774e-02  1.004e-05  1.228e-02  1.151e-05  1.922e-02  5.570e-01 -9.440e+00  9.470e+0
-7.947e-05  2.064e-02  4.539e-03 -4.434e-05  7.897e-05  1.102e-04  3.129e-04  1.686e-04  4.581e-07  1.366e-04 -7.749e-08
-7.947e-05  2.064e-02  4.539e-03 -4.434e-05  7.897e-05  1.102e-04  3.129e-04  1.686e-04  4.581e-07  1.366e-04 -7.749e-08 -2.215e-04 -2.007e-02 -2.765e-01 -1.111e-0
 1.874e-02 -1.105e+01 -4.415e-01  6.591e-03 -2.133e-02 -9.662e-04  3.403e-02 -4.271e-03  1.892e-04  3.910e-03  5.929e-05
 1.874e-02 -1.105e+01 -4.415e-01  6.591e-03 -2.133e-02 -9.662e-04  3.403e-02 -4.271e-03  1.892e-04  3.910e-03  5.929e-05 -8.535e-02  2.754e+00  6.666e+01  1.342e+0
-7.264e-05  2.154e-02  3.184e-03 -3.601e-05  7.100e-05  5.026e-05  7.972e-05  9.479e-05 -1.053e-07  5.712e-05 -1.236e-07
-7.264e-05  2.154e-02  3.184e-03 -3.601e-05  7.100e-05  5.026e-05  7.972e-05  9.479e-05 -1.053e-07  5.712e-05 -1.236e-07  5.130e-05 -1.979e-02  4.008e-01 -1.315e-0
-4.196e-04 -1.163e+01  2.364e-01 -6.384e-03 -1.878e-02 -3.226e-02 -1.017e-01 -3.702e-03 -1.295e-04 -2.918e-02  4.846e-05
-4.196e-04 -1.163e+01  2.364e-01 -6.384e-03 -1.878e-02 -3.226e-02 -1.017e-01 -3.702e-03 -1.295e-04 -2.918e-02  4.846e-05  9.834e-02  8.133e+00 -4.549e+01 -8.526e+0
PARAMETER  CORRELATION COEFFICIENTS
      NO.  GLOBAL      6     14     17     18     19     20     25     26     27     28     29     30     31     36     37     38
       6  0.45278   1.000 -0.001 -0.223  0.067 -0.060 -0.043 -0.008  0.034  0.277 -0.351  0.271 -0.349 -0.013  0.000 -0.001 -0.001
      14  0.35897  -0.001  1.000 -0.010  0.021  0.038  0.033  0.000 -0.000 -0.001  0.000 -0.000  0.000 -0.223 -0.008  0.034  0.166
      17  0.56317  -0.223 -0.010  1.000 -0.519  0.178  0.148  0.006  0.016 -0.036  0.023 -0.034  0.019  0.191 -0.003  0.008  0.006
      18  0.66582   0.067  0.021 -0.519  1.000 -0.287 -0.171  0.000 -0.022  0.001 -0.003 -0.001 -0.009 -0.378  0.007 -0.016 -0.009
      19  0.85108  -0.060  0.038  0.178 -0.287  1.000  0.826  0.009  0.007 -0.011  0.004 -0.009  0.008 -0.173  0.004  0.004  0.008
      20  0.83259  -0.043  0.033  0.148 -0.171  0.826  1.000  0.019  0.008 -0.000  0.006 -0.007 -0.006 -0.138  0.011  0.003  0.015
      25  0.81296  -0.008  0.000  0.006  0.000  0.009  0.019  1.000  0.054 -0.309  0.136  0.288 -0.109 -0.002  0.000  0.000  0.000
      26  0.53953   0.034 -0.000  0.016 -0.022  0.007  0.008  0.054  1.000 -0.257  0.039 -0.240 -0.018  0.009 -0.000  0.000  0.000
      27  0.93176   0.277 -0.001 -0.036  0.001 -0.011 -0.000 -0.309 -0.257  1.000 -0.820  0.729 -0.684  0.004  0.000  0.000  0.000
      28  0.86427  -0.351  0.000  0.023 -0.003  0.004  0.006  0.136  0.039 -0.820  1.000 -0.712  0.682  0.001  0.000  0.000  0.000
      29  0.92753   0.271 -0.000 -0.034 -0.001 -0.009 -0.007  0.288 -0.240  0.729 -0.712  1.000 -0.775  0.003 -0.000  0.000 -0.000
      30  0.83497  -0.349  0.000  0.019 -0.009  0.008 -0.006 -0.109 -0.018 -0.684  0.682 -0.775  1.000  0.000 -0.000  0.000 -0.000
      31  0.52654  -0.013 -0.223  0.191 -0.378 -0.173 -0.138 -0.002  0.009  0.004  0.001  0.003  0.000  1.000 -0.000  0.004 -0.027
      36  0.81224   0.000 -0.008 -0.003  0.007  0.004  0.011  0.000 -0.000  0.000  0.000 -0.000 -0.000 -0.000  1.000 -0.053 -0.295
      37  0.48252  -0.001  0.034  0.008 -0.016  0.004  0.003  0.000  0.000  0.000  0.000  0.000  0.000  0.004 -0.053  1.000 -0.222
      38  0.90295  -0.001  0.166  0.006 -0.009  0.008  0.015  0.000  0.000  0.000  0.000 -0.000 -0.000 -0.027 -0.295 -0.222  1.000
      39  0.82319   0.000 -0.202 -0.001  0.003 -0.005 -0.000  0.000 -0.000  0.000  0.000  0.000 -0.000  0.008  0.161  0.061 -0.792
                    1.000 -0.624  0.593
      40  0.91006  -0.001  0.158  0.004 -0.006  0.007  0.006  0.000  0.000 -0.000  0.000 -0.000  0.000 -0.024  0.390 -0.239  0.639
                   -0.624  1.000 -0.725
      41  0.79832  -0.000 -0.258  0.001 -0.003 -0.005 -0.012 -0.000 -0.000 -0.000 -0.000  0.000  0.000  0.030 -0.134 -0.047 -0.614
                    0.593 -0.725  1.000
```

Summary:

$\tau(B^0) = 453.3 \pm 15.6$ μm
$\tau(B^0) = 482.2 \pm 14.6$ μm

Resolution function:
$g = 0.58 \pm 0.15$
$\tau_{\rm r} = 0.63 \pm 0.19$
$s = 1.39 \pm 0.10$ (scale factor)

Figures 26 and 27 show the Δz distributions for charged and neutral B candidates in the signal regions. As discussed in section 8, we use an approximation that makes it possible to calculate Δt from Δz. The equivalent plots as a function of Δt are in figures 28 and 29. Note that $\Delta z \to -\Delta t$ to use the same conventions as other analyses.

The resolution function obtained from Monte Carlo and the above result of the lifetime fit are compared in figure 30. The black histogram represents the resolution function obtained from signal Monte Carlo. A fit of the "$G + G \otimes E$" parameterisation is superimposed (black line). The red curve is the resolution function from the lifetime fit on data as quoted above. The two curves are normalised to the same surface.

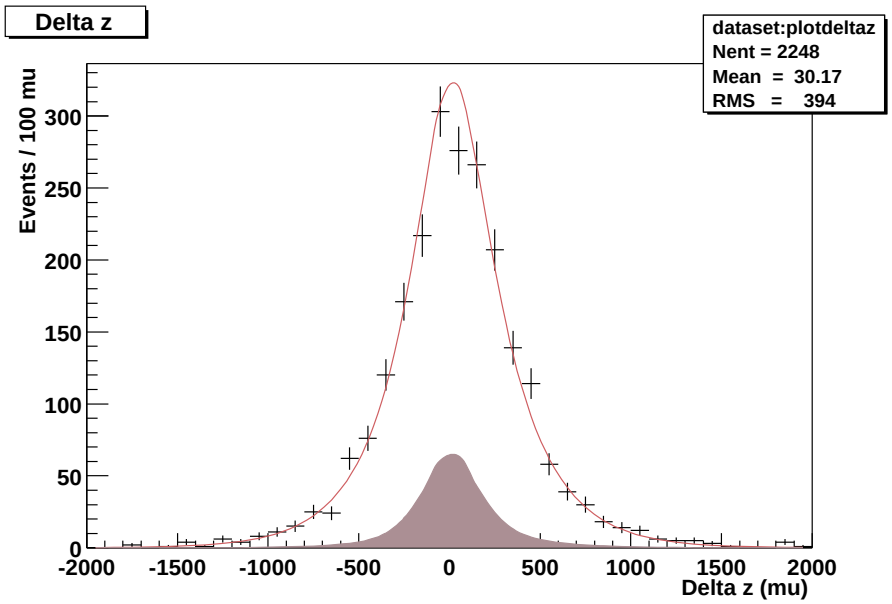

Figure 26: Δz distribution for $B^0/\overline{B}^0$ candidates in the signal region. The result of the lifetime fit is superimposed.

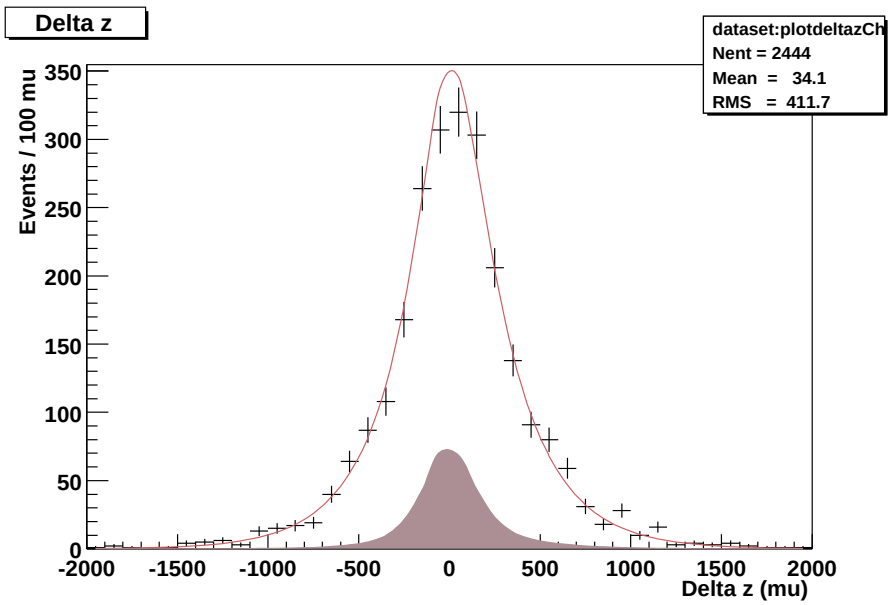

Figure 27: Δz distribution for $B^{\pm}$ candidates in the signal region. The result of the lifetime fit is superimposed.

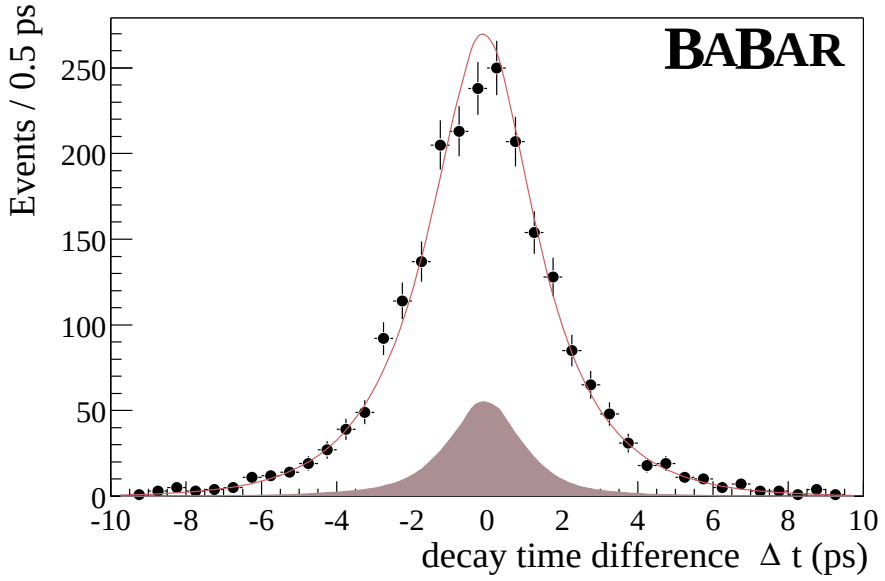

Figure 28: An equivalent way of making the plot in figure 26.

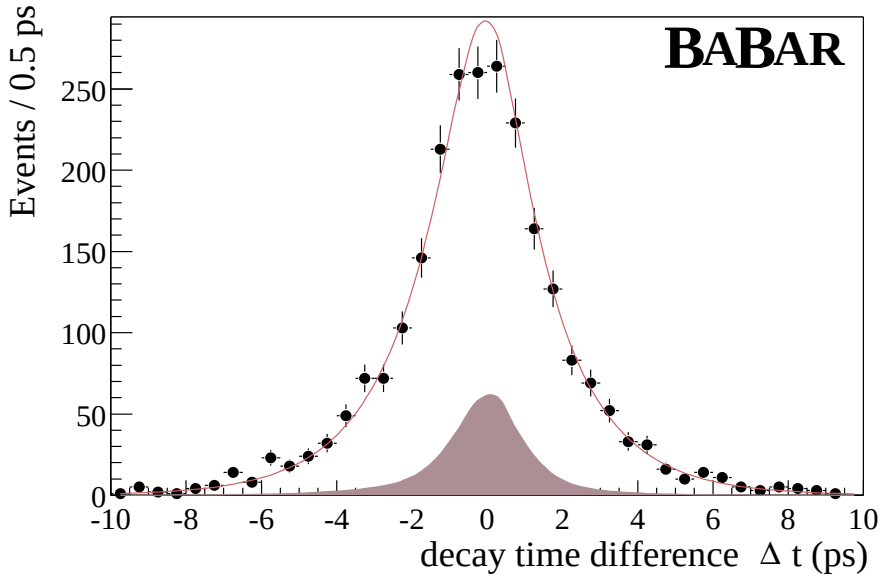

Figure 29: An equivalent way of making the plot in figure 27.

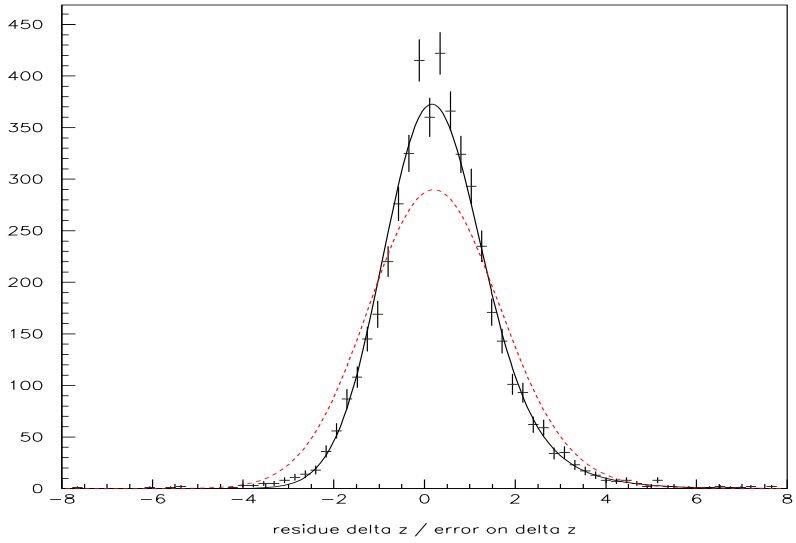

Figure 30: Comparison of the Δz resolution function extracted from the lifetime fit (red) and signal Monte Carlo (black).

11 Consistency checks in data

Split the data sample in bins of different variables like

- $B_{\rm rec}$ decay mode
- ϕ angle of the charmed meson from the fully reconstructed B,
- ϕ angle of the hard pion from the fully reconstructed B,
- data sets / run numbers,
- event number within a run.

Is the charm lifetime accurately measured in the $B_{\rm rec}$ decay samples... ?

12 Systematic uncertainties

The decay length difference technique is different from various other methods used in other experimental environments, e.g. at SLD, LEP and CDF [refs.]. For example, the measurement is made in z rather than in the transverse plane, and the production point of the B mesons is unknown. Consequently, some of the systematic uncertainties are also different.

The systematic uncertainties in our B meson lifetime measurements can be grouped in three categories: uncertainties due to (1) the selection criteria used to obtain the data samples, (2) the Δz reconstruction and (3) the fitting procedure.
The first category is discussed in section 12.1, the second one in sections 12.4-12.7 and the third one on sections 12.8-12.12. The systematic uncertainties are summarised and combined in section 12.13.

12.1 Sample selection

In general, selection criteria can bias the decay time distribution of candidates in the final sample. For example, quality cuts can produce such an effect if candidates with long decay times reach regions in the detector where the spatial resolution is significantly worse than at the interaction region. We do not expect this particular effect to be large for Bs in *BABAR*.

We perform several tests on the generated Δz spectrum of candidates selected from all available signal Monte Carlo. We calculate the average Δz for the B^0 sample and the B^+ sample. Both are consistent with zero (table 10). We perform unbinned maximum likelihood fits of the theoretical Δz distribution to the spectra of the two samples. The fitted lifetimes (table 10) are consistent with the generated lifetimes. We use the result of the likelihood fit and binned histograms of the Δz spectra of the samples to calculate a χ^2 (table 10).
These two tests do not show any evidence of a significant distortion of the Δz spectrum.

We use our combined fitting procedure, excluding background modelling, to extract the lifetime from the distributions of reconstructed Δz for the two samples. The fitted lifetimes (table 10) are consistent with the generated ones. We assign the statistical error from these fits as systematic uncertainty on our measurements on data ("MC statistics" in table 14).

		using generated Δz			using reconstructed Δz
	generated lifetime	average Δz	fitted lifetime	χ^2/ndof	fitted lifetime
B^0	468 μm	-3.4 ± 2.9 μm	464.8 ± 3.6 μm	128.9/149	476.6 ± 4.7 μm
B^+	486 μm	0.7 ± 2.2 μm	487.4 ± 2.9 μm	171.6/149	490.7 ± 4.2 μm

Table 10: Checks of B decay time spectra and reconstruction/selection procedure.

12.2 Parameterisation of the resolution function

In measurements that use the decay length difference technique, the lifetime to be measured is strongly correlated to the resolution function. In this measurement, the largest systematic error comes from the the fact that our knowledge of the Δz resolution in data is limited. We "transform a part of this systematic uncertainty into a contribution to the statistical error" by letting all parameters in the resolution function free during the lifetime fit. This uncertainty is already included in our statistical error. For illustration purposes, we repeat the combined lifetime fit fixing the parameters in the resolution function at the values obtained in the fit discussed section 10. The error on $\tau(B^0)$ ($\tau(B^+)$) is reduced from 15.6 μm (14.6 μm) to 13.3 μm (12.8 μm). The "difference in quadrature" is 8.2 μm (6.9 μm) or 1.8 % (1.4%).

Additional uncertainties arise from the possibility that the parameterisation of the resolution function, despite its free parameters, is not "flexible" enough to reproduce all features of the "real" resolution function. A comparison of different parameterisations is discused in section 8.5. The differences in the column "Fixed resolution function" of table 8 are due to the different forms and flexibilities of the parameterisations. We attribute the difference between the lifetimes obtained with $G + G \otimes E$ and $G_1 + G_2$ as systematic uncertainty on the lifetimes obtained with $G + G \otimes E$.

12.3 Identical resolution function

We use a combined fit to the Δz distributions of charged and neutral Bs (section 8.4). For this fit, we make the approximation of equal resolution functions for all $B_{\rm rec}$ modes, regardless of the B species. To estimate the size of the error introduced by this approximation, we generate toy Monte Carlo samples with different resolution functions for charged and neutral Bs and we use the combined fit to extract the two lifetimes.
We simulate 1400 experiments, each with roughly the statistics that we have in data. The values for $B^- \to J/\psi K^-$ and $\overline{B}^0 \to D^{*+}\pi^-$ from table 5 are used to model the resolution functions at generation time. The bias $\tau_{\rm generated} - \tau_{\rm reconstructed}$ on the fitted $\tau(B^0)$ ($\tau(B^+)$) is

-1.3 ± 0.4 μm (1.5 ± 0.4 μm). We assign 1.5 μm as systematic error on the two lifetimes we measure in data.

12.4 Beam spot

VtxTagBtaSelFit, the algorithm we use to reconstruct Δz, makes use of the beam spot position and size to obtain a constraint on the opposite vertex (see section 6.3). A potential bias in the determination of the beam spot [22] can change the Δz resolution function.
We use Monte Carlo events to estimate the magnitude of this effect. Figure 31 shows a comparison of the Δz pull for the same set of events reconstructed twice with different estimates of the beam spot position. The y dimension of the beam spot is of the order of 10 μm [23], and in x it is roughly ten times larger. For the Δz reconstruction we use, both on data and on Monte Carlo, an "effective beam spot" size of around 40 μm in y that includes effects of the actual beam spot size and the finite precision of our determination of the beam spot parameters.
The black points in figure 31 represent the Δz pull obtained from 4.2k B^0 events reconstructed with the standard beam spot. For the second reconstruction of the same events we shift the beam spot position by 80 μm in y. The corresponding Δz pull is represented by the red points in figure 31. The values for the parameters of the $G + G \otimes E$ parameterisation extracted from a fit to these histograms are compared in table 11. The effect is small and our parameterisation of the resolution function can account for it. We do not assign a systematic error.

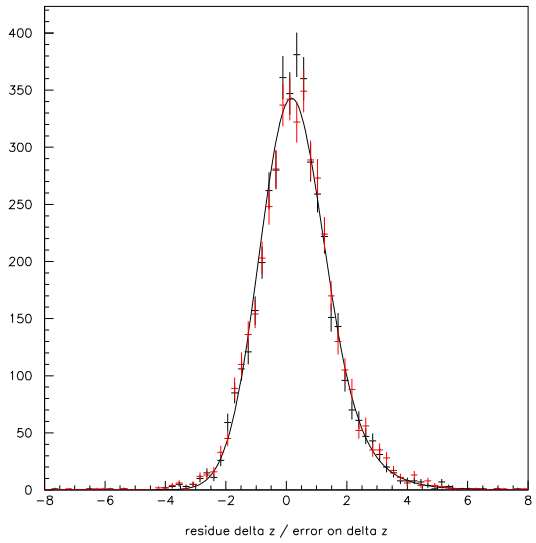

Figure 31: Δz pull for the same set of events reconstructed twice; once using the generated beam spot position (black) and once (red) using a biased estimate of the beam spot position (shifted 80 μm in y).

	standard beam spot	shifted beam spot
number of reconstructed events	4228	4218
g	0.611 ± 0.033	0.602 ± 0.034
s	1.008 ± 0.018	1.042 ± 0.017
$\tau_{\rm r}$	0.860 ± 0.059	0.884 ± 0.064
χ^2/ndof	73.6/48	57.7/48

Table 11: Fits of the $G+G\otimes E$ parameterisation to the diffent pull distributions in figure 31.

12.5 Momentum of the fully reconstructed B

The estimation of the $B_{\rm rec}$ "pseudo-track" (section 6.3) not only relies on the beam spot, but also on the reconstructed $B_{\rm rec}$ momentum. We use the same technique as above to estimate the effect of a possible bias in the $B_{\rm rec}$ momentum reconstruction, comparable in size to the resolution (e.g. $\sigma(p_x) = 15$ MeV, $\sigma(p_y) = 15$ MeV and $\sigma(p_z) = 17$ MeV for $\overline{B}^0 \to D^{*+}\rho^-$). We do not observe any significant change in the values of parameters in the resolution function. The error on the $B_{\rm opp}$ flight direction introduced by such a momentum bias is small compared to the error introduced by an 80 μm shift of the beam spot y position.

12.6 Δz outliers

The likelihood function for the lifetime fit contains a term that models the effect of outliers (see figure 19, sections 6.4.3 and 8.3). The fractions of outliers in the B^0 and the B^+ samples are free parameters in the lifetime fit. We cut at $|\Delta z| < 3000\mu$m. We assume a Δz distribution with zero mean and a width of 2500 μm for the outliers. If we change the width of this gaussian to 4000 μm, the central value for $\tau(B^0)$ ($\tau(B^+)$) gets 4.9 μm (6.1 μm) higher. Figure 19 might indicate that the Δz distribution for outliers is not centered at zero. If we change the mean of the outlier-gaussian to 1000 μm, the central value for $\tau(B^0)$ ($\tau(B^+)$) gets 0.4 μm (2.6 μm) higher. We assign 4.9 μm (6.1 μm) as systematic uncertainty.

12.7 Detector geometry and alignment

Imperfections in the detector alignment can influence the Δz reconstruction. We study random misalignments of SVT wafers, "squeezing" of the SVT (reducing its radius) and translations of the SVT with respect to the DCH. *BABAR* Monte Carlo events are simulated with perfect alignment. We reconstruct the same 10k $\overline{B}^0 \to D^{*+}\pi^-$ events several times with diffent misalignments introduced into a conditions database proxy:

- **Zero:** Perfect alignment.
- **LA101025:** Uncorrelated random translations of all SVT wafers. The translations in u (parallel to the beam axis) and v (in the wafer plane, normal to u) are normally distributed with $\sigma = 10$ μm. The translations in w are normally distributd with

$\sigma = 25$ μm. This model is believed to roughly reproduce the effects of the residual misalignment on our sample of real data [24].

- **LA202050:** As above, but with $\sigma = 20$ μm in u and v, and $\sigma = 50$ μm in w.
- **Trans100:** The SVT as a whole is translated by 100 μm in x with respect to the DCH. This is significantly more than the relative drift between two subsequent calibrations [25]. The impact of a relative translation in z is expected to be smaller than the effect of an x translation, because of the different DCH resolutions in these directions.
- **Squeeze:** Reduce the radius of the SVT. The radius of each layer is reduced by an amount proportional to its radius. The radius of the outermost layer is reduced by 15 μm.

The average Δz bias and resolutions (weighed means over two gaussians) are summarised in table 12. It also contains the results of fits of the $G + G \otimes E$ parameterisation to the different pull distributions.
As expected, the misalignments under study can degrade the Δz resolution and change the average bias, as well as broaden the pull distributions. The χ^2 values in the last row of table 12 indicate that the $G + G \otimes E$ parameterisation of the Δz resolution function is flexible enough to reproduce the effects. The values of the parameters change, but the same functional form gives a comparable χ^2 value. Fits to the Δz pull distributions for Zero and LA202050 are shown in figure 32.

The parameters of the resolution function are free in the lifetime fit. We do not assign a systematic error due to misalignment effects.

Various alignment and calibration procedures use data to correct for relative displacements of different detector components. These procedures do not determine or adjust the global length scale of the experiment. In the same way as a bias in the boost determination, a possible imperfection in the z scale of the detector directly biases the B lifetime measurements. One way to determine the z scale is to use the detector to measure the length in z of something with known dimensions. Such a measurement of the length of the Be beam pipe [23] using protons from material interactions therein [26] is currently underway. A preliminary measurement [27] of this length gives 180.38 ± 0.53 mm, to be compared to the 180.09 mm obtained from an independent measurement.
Until these results are better documented, we use a very crude estimate of the maximum uncertainty one could expect. To minimise mechanical force on the fragile SVT modules they are mounted in a way that allows them to move in order to avoid the force exerted by deformations of the support structure. Relative movements of one module with respect to another one are corrected by the local alignment procedure. The physical size of individual wafers is known within a precision of the oder of 50 μm [28]. It is unlikely that the precision of the process of glueing wafers together to make a module (glue four to eight wafers to a mechanical support) is less precise than 1 mm over the whole length of $\simeq 10$ cm [29]. This

		Zero	LA101025	LA202050	Trans100	Squeeze
Δz residue:	bias (μm)	32.8 ± 2.4	34.0 ± 2.5	38.2 ± 2.9	29.1 ± 2.4	29.2 ± 2.3
	resolution (μm)	135.6 ± 2.6	148.4 ± 2.5	168.7 ± 2.6	135.9 ± 2.2	134.3 ± 2.1
	χ^2	1.51	0.99	0.96	1.37	1.55
Δz pull:	g	0.637 ± 0.033	0.607 ± 0.037	0.539 ± 0.057	0.712 ± 0.029	0.712 ± 0.029
	s	1.060 ± 0.018	1.124 ± 0.018	1.327 ± 0.025	1.071 ± 0.017	1.067 ± 0.017
	$\tau_{\rm r}$	0.925 ± 0.067	0.919 ± 0.071	0.816 ± 0.092	1.045 ± 0.079	1.064 ± 0.083
	χ^2	1.35	1.10	1.11	1.05	1.15

Table 12: Results of fits to the Δz residue and pull for reconstruction with various misalignments.

corresponds to a z scale uncertainty of $\simeq 1$ mm/10 cm $= 1$ % which we assign as sytematic error.

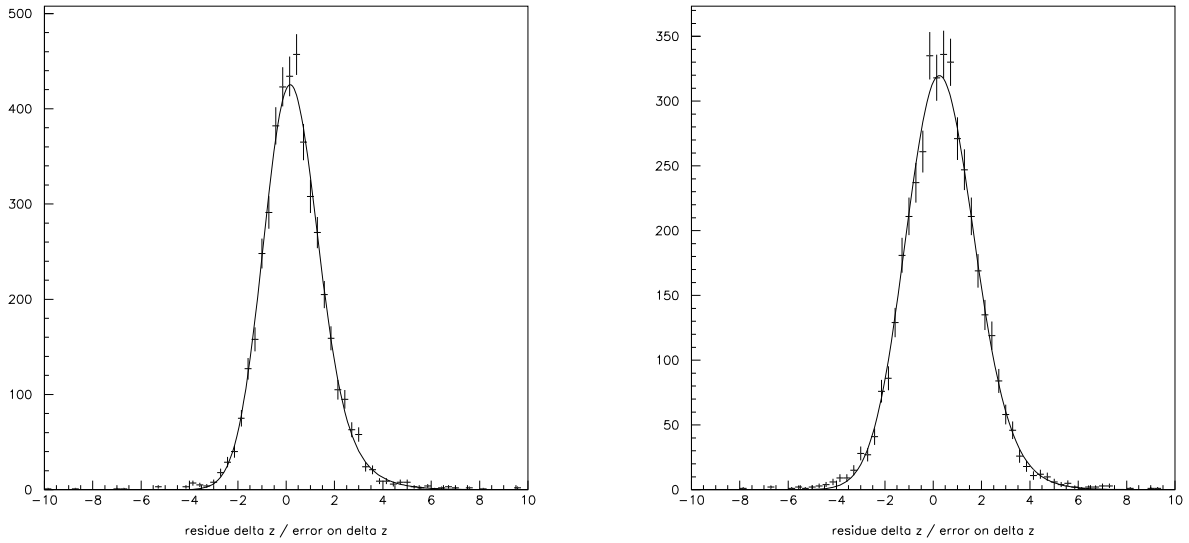

Figure 32: Δz pull for perfect alignment (Zero, left plot) and for poorly aligned SVT (LA202050, right plot).

12.8 Average boost approximation

We use the boost of the $\Upsilon(4S)$ as approximation for the boost of the Bs. The effect of this approximation does not average out completely. The author of [30] uses analytical calculations to show that this approximation results in a 0.4 % overestimation of the lifetime. We obtain compatible results in toy Monte Carlo studies. We correct our measurements for this bias and assign 0.4 % as systematic uncertainty.

12.9 Uncertainty on the average boost

The lifetime measurements are performed in z, the direction of the boost. A possible bias on the measured boost directly biases the lifetime: bias(τ_B) $\propto$ bias($(\beta_z\gamma)_{\Upsilon(4S)}$). This can be seen from the first formula in section 8.1.

OPR measures $\vec{\beta}_{\Upsilon(4S)}$ from 2-prongs. The accuracy on $(\beta_z\gamma)_{\Upsilon(4S)}$ is better than 0.3 % [31]. We assign $\sqrt{(0.4\ \%)^2 + (0.3\ \%)^2}$ as total uncertainty on the lifetimes due to the average boost approximation and determination.

12.10 Signal probability

Our fits to the substituted mass spectra come with covariance matrices. We repeat the lifetime fit varying the value of the (fixed) parameters that describe the substituted mass spectra within 2σ of the result of the independent fits to these spectra. The central value of the B^0 (B^+) lifetime changes by 0.9 μm (0.7 μm) if we vary the fraction of events in the signal gaussian; and significantly less if we vary the other parameters.

We reconstruct B^0s in modes including a ρ resonance (see section 4). To estimate the impact of a possible tail of the signal $m_{\rm SE}$ distribution, we repeat the lifetime fit using a different function to model the $m_{\rm SE}$ spectrum for B^0s. Instead of "Argus+Gaussian" we use "Argus+Johnson S_U distribution". For a certain choice of parameters, the latter distribution tends towards a gaussian, but it can also model a tail. The central value of the B^0 lifetime changes by 0.1 μm.

We assign 0.9 μm (0.7 μm) as systematic uncertainty.

12.11 Background modelling

We run the same reconstruction procedure on all available generic Monte Carlo [14]. The substituted mass spectra, including a break-down of the different contributions to the background are shown in figures 5 and 6. The background compositions in the mass sideband and in the signal region are summarised in table 13 [14]. The Δz distributions for background events in the signal region and in the sideband region are compared in figures 33 and 34. For candidate $B^0/\overline{B}^0$ events, the background compositions in the signal and sideband regions are compatible. The corresponding Δz distributions (figure 33) agree fairly well. For candidate $B^\pm$ events, there is a significant discrepancy in the background compositions in the signal and sideband regions. The available statistics of background events is low. Figure 34 contains a hint that the tail at positive Δz can be longer for background candidates "under the peak". As we use sideband events to extract the Δz distribution of the background, this is a potential source of bias.

We use toy Monte Carlo samples generated with different Δz distributions for the background in the sideband and signal regions to estimate the size of the effect. The generated

Δz distributions for the sideband region are identical to the fits shown in figures 23 and 24. In the signal region, we increase the "lifetime" of the exponential at positive Δz and the fraction of events in this tail. For charged Bs, we increase the "lifetime" by 150 μm and the fraction by 5 %. For neutral Bs we use one third of these values. The bias $\tau_{\rm generated} - \tau_{\rm reconstructed}$ on the fitted $\tau(B^+)$ ($\tau(B^0)$) estimated from 1000 simulated experiments is -5.1 ± 0.6 μm (-1.6 ± 0.5 μm). We assign 5.1 μm (1.6 μm) as systematic uncertainty due to the background model.

		Same B species	Other B species	$c\overline{c}$	$uds/\overline{uds}$
B^0:	Sideband ($5.2 < M_{\rm ES} < 5.26$)	30.9 ± 1.5 %	12.3 ± 1.0 %	44.9 ± 1.6 %	11.9 ± 1.0 %
	Signal ($M_{\rm ES} > 5.275$)	36.3 ± 3.3 %	18.9 ± 2.7 %	37.3 ± 3.3 %	7.5 ± 1.8 %
B^+:	Sideband ($5.2 < M_{\rm ES} < 5.26$)	12.1 ± 1.4 %	8.2 ± 1.2 %	67.3 ± 2.0 %	12.5 ± 1.4 %
	Signal ($M_{\rm ES} > 5.275$)	33.6 ± 4.5 %	23.6 ± 4.1 %	39.1 ± 4.7 %	3.4 ± 1.8 %

Table 13: Break-down of the background contributions.

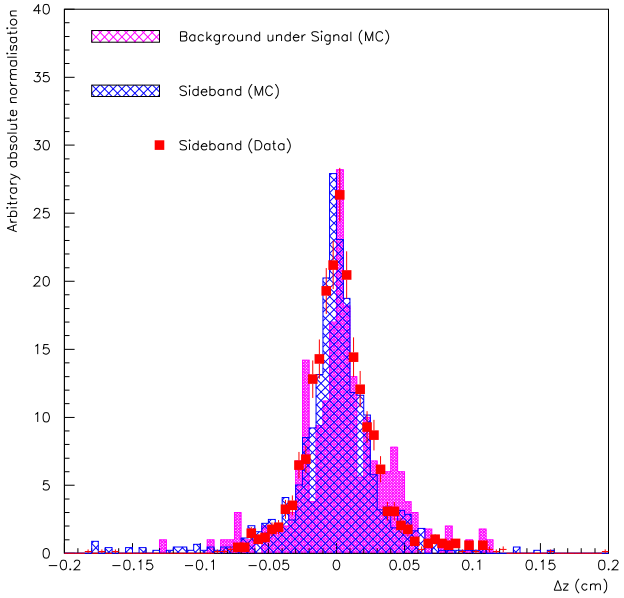

Figure 33: Δz distributions for background B^0 candidates in the signal and sideband regions.

12.12 Monte Carlo test of fitting procedure

A test of our fitting procedure and its technical implementation is reported in section 8.5 (see table 7). This test gives an estimate of a possible bias on the fitted lifetime of -1.1 ± 0.7 μm and -1.8 ± 0.8 μm for neutral and charged Bs, respectively. These values are consistent

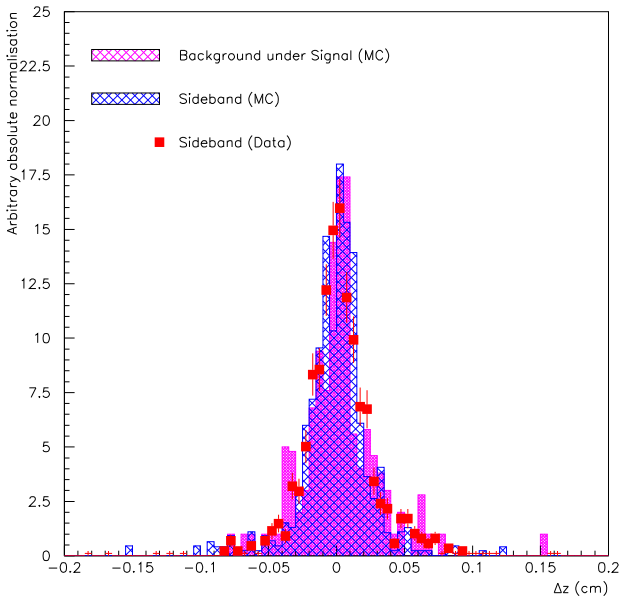

Figure 34: Δz distributions for background B^+ candidates in the signal and sideband regions.

with zero, within a statistical error that is small compared to the uncertainties due to the reconstruction procedure (section 12.1). We do not assign a systematic error due to the fitting procedure.

12.13 Total systematic uncertainty

A summary of all systematic errors as well as their sum (in quadrature) is given in table 14.

13 Lifetime ratio

We replace the two lifetimes in our fit by the B^0 lifetime and the the ratio $r = \frac{\tau(B^+)}{\tau(B^0)}$.

13.1 Fit result

Parameters:
1-5: mass spectrum B0
6-8: outliers B0
(fraction in per mil)
9-13: mass spectrum B+
14-16: outliers B+

systematic effect	uncertainty on $\tau(B^0)$ (μm)	uncertainty on $\tau(B^+)$ (μm)
MC statistics	4.7	4.2
Parameterisation of resolution function	1.5	1.5
One single resolution function	1.5	1.5
Δz outliers	4.9	6.1
z scale	4.5	4.8
Boost	1.8	1.9
Signal probability	0.9	0.7
Background modelling	1.6	5.1
Total in quadrature	8.8	10.6

Table 14: Summary of the systematic errors in the B lifetime measurements.

(fraction in per mil)
17: lifetime B0
18: lifetime ratio r
19-21: resolution function
22-25: error spectrum B0
26-31: background B0
32-35: error spectrum B+
37-41: background B+

```
MIGRAD MINIMIZATION HAS CONVERGED.
MIGRAD WILL VERIFY CONVERGENCE AND ERROR MATRIX.
COVARIANCE MATRIX CALCULATED SUCCESSFULLY
FCN=95037.4 FROM MIGRAD    STATUS=CONVERGED     854 CALLS         855 TOTAL
                     EDM=0.0299064    STRATEGY= 2      ERROR MATRIX ACCURATE
 EXT PARAMETER                                   STEP         FIRST
 NO.   NAME      VALUE            ERROR          SIZE      DERIVATIVE
  1  endptB0      5.29000e+00   constant
  2  cB0         -3.44000e+01   constant
  3  bmassB0      5.27992e+00   constant
  4  bresnB0      2.77400e-03   constant
  5  fB0          4.85300e-01   constant
  6  outFracB0    2.40360e+00   2.01701e+00   3.82399e-01  -1.12371e-03
  7  outWidthB0   2.50000e+03   constant
  8  outMeanB0    0.00000e+00   constant
  9  endptCh      5.29000e+00   constant
 10  cCh         -3.17000e+01   constant
 11  bmassCh      5.27961e+00   constant
 12  bresnCh      2.65500e-03   constant
 13  fCh          5.86700e-01   constant
 14  outFracCh    5.37382e+00   2.40517e+00   4.78129e-01   8.72971e-04
 15  outWidthCh   2.50000e+03   constant
 16  outMeanCh    0.00000e+00   constant
 17  tauB0        4.53576e+02   1.64557e+01   1.82167e+00  -4.56705e-04
 18  tauBFrac     1.06535e+00   4.38480e-02   5.61175e-03  -4.35287e-01
 19  sigma        1.38762e+00   9.94186e-02   1.57268e-02  -1.11010e-01
 20  tau          6.53321e-01   2.34177e-01   2.23970e-02   6.19499e-01
 21  frac         5.92831e-01   1.62132e-01   1.67038e-02   1.56280e-01
 22  mperrB0      8.13000e+01   constant
 23  errmsB0      1.51000e+01   constant
 24  errp1B0     -2.88000e-01   constant
 25  errp2B0      1.64000e+01   constant
 26  coremeanB0   7.45308e+00   1.77482e+01   2.19187e+00   1.01149e-03
 27  corewidthB0   1.57778e+02   1.05775e+01   1.88818e+00   1.40474e-03
 28  posfracB0    3.37125e-01   5.69786e-02   4.39330e-03   5.20275e-01
 29  postauB0     2.43216e+02   2.20319e+01   2.36069e+00   2.91578e-04
 30  negfracB0    2.84388e-01   5.22599e-02   4.14987e-03  -8.95640e-02
 31  negtauB0     2.12061e+02   1.95370e+01   2.29255e+00   1.84232e-04
```

```
 32  mperrCh      7.17000e+01   constant
 33  errmsCh      1.17100e+01   constant
 34  errp1Ch     -2.31000e-01   constant
 35  errp2Ch      3.10000e+01   constant
 36  coremeanCh  -3.13389e+00   1.81881e+01   2.26015e+00  -1.01729e-04
 37  corewidthCh   1.43284e+02   9.71498e+00   1.81339e+00  -7.05149e-05
 38  posfracCh    3.29734e-01   5.13459e-02   4.69973e-03  -3.84624e-02
 39  postauCh     2.44745e+02   2.26993e+01   2.74409e+00   6.68632e-05
 40  negfracCh    2.89265e-01   5.64053e-02   4.98223e-03  -1.68977e-02
 41  negtauCh     1.91928e+02   1.86713e+01   2.39128e+00   1.43802e-05
                           ERR DEF= 0.5
EXTERNAL ERROR MATRIX.    NDIM=  41    NPAR= 19    ERR DEF=0.5
ELEMENTS ABOVE DIAGONAL ARE NOT PRINTED.
 4.068e+00
 9.775e-03  5.785e+00
-7.569e+00 -7.266e-01  2.708e+02
 1.595e-02 -1.541e-02 -5.062e-01  1.923e-03
 1.208e-02  7.524e-03 -7.602e-01  4.609e-04  9.884e-03
 4.174e-03  6.113e-03 -4.979e-01  3.542e-04 -5.750e-03  5.484e-02
 4.521e-03  4.085e-03 -3.041e-01  2.543e-04 -2.466e-03  3.300e-02  2.629e-02
-2.482e-01  7.319e-03  7.751e-01 -2.440e-03  5.414e-04  4.180e-02  5.261e-02  3.150e+02
 7.411e-01 -1.888e-02  2.609e+00 -2.700e-03 -2.364e-02  1.089e-02  1.054e-02  9.976e+00  1.119e+02
 3.200e-02 -1.114e-05 -3.501e-02  8.439e-05 -2.615e-06  2.622e-05  8.409e-05 -3.097e-01 -1.528e-01  3.247e-03
-1.567e+01 -7.330e-03  8.767e+00 -1.906e-02 -5.608e-03 -1.857e-02 -3.609e-03  5.205e+01  8.422e+00 -1.030e+00  4.854e+02
 2.873e-02 -1.197e-05 -3.067e-02  7.349e-05 -1.041e-05  2.774e-05  2.236e-05  2.687e-01 -1.309e-01  2.173e-03 -8.207e-01
 2.873e-02 -1.197e-05 -3.067e-02  7.349e-05 -1.041e-05  2.774e-05  2.236e-05  2.687e-01 -1.309e-01  2.173e-03 -8.207e-01  2.731e-03
-1.380e+01 -8.207e-03  6.193e+00 -1.348e-02 -1.606e-02  9.929e-03 -2.969e-02 -3.823e+01 -4.300e+00 -7.623e-01  2.942e+02
-1.380e+01 -8.207e-03  6.193e+00 -1.348e-02 -1.606e-02  9.929e-03 -2.969e-02 -3.823e+01 -4.300e+00 -7.623e-01  2.942e+02 -7.924e-01  3.817e+02
 2.571e-02 -3.873e-01 -1.389e+00  3.147e-03  1.309e-02  2.657e-02  3.685e-02  1.102e-01 -1.385e-02  2.212e-04  3.149e-03
 2.571e-02 -3.873e-01 -1.389e+00  3.147e-03  1.309e-02  2.657e-02  3.685e-02  1.102e-01 -1.385e-02  2.212e-04  3.149e-03  2.140e-05 -1.243e-01  3.308e+02
-1.932e-02  7.862e-01  1.248e+00 -1.497e-03 -1.534e-02  6.240e-03  3.366e-03  2.024e-03  3.803e-02  1.489e-05  1.155e-02
-1.932e-02  7.862e-01  1.248e+00 -1.497e-03 -1.534e-02  6.240e-03  3.366e-03  2.024e-03  3.803e-02  1.489e-05  1.155e-02  1.567e-05  1.863e-02 -9.133e+00  9.438e+0
-3.927e-05  2.058e-02  3.401e-03 -5.140e-05 -3.695e-05  4.319e-05  8.361e-05  2.767e-04  1.495e-04  6.504e-07  9.904e-05
-3.927e-05  2.058e-02  3.401e-03 -5.140e-05 -3.695e-05  4.319e-05  8.361e-05  2.767e-04  1.495e-04  6.504e-07  9.904e-05  8.497e-08 -2.641e-04 -2.785e-01 -1.123e-0
 4.851e-03 -1.102e+01  4.905e-02  5.917e-03  5.887e-03 -2.372e-02 -1.956e-03  3.443e-02 -9.507e-04  1.222e-04  2.009e-02
 4.851e-03 -1.102e+01  4.905e-02  5.917e-03  5.887e-03 -2.372e-02 -1.956e-03  3.443e-02 -9.507e-04  1.222e-04  2.009e-02  1.389e-06 -7.479e-02  6.762e+01  1.401e+0
-3.550e-05  2.149e-02  2.120e-03 -4.806e-05 -2.889e-05  3.607e-05  2.623e-05  4.587e-05  7.584e-05  6.628e-08  2.403e-05
-3.550e-05  2.149e-02  2.120e-03 -4.806e-05 -2.889e-05  3.607e-05  2.623e-05  4.587e-05  7.584e-05  6.628e-08  2.403e-05  2.102e-08  1.267e-05  3.984e-01 -1.322e-0
-1.417e-02 -1.164e+01  6.457e-01  1.644e-02 -9.202e-03 -7.472e-03 -2.409e-02 -9.019e-02  3.799e-03 -1.936e-04 -1.607e-02
-1.417e-02 -1.164e+01  6.457e-01  1.644e-02 -9.202e-03 -7.472e-03 -2.409e-02 -9.019e-02  3.799e-03 -1.936e-04 -1.607e-02 -5.860e-06  1.130e-01 -4.517e+01 -8.134e+0
PARAMETER  CORRELATION COEFFICIENTS
      NO.  GLOBAL      6     14     17     18     19     20     21     26     27     28     29     30     31     36     37     38
       6  0.45610   1.000  0.002 -0.228  0.180  0.060  0.009  0.014 -0.007  0.035  0.278 -0.353  0.273 -0.350  0.001 -0.001 -0.000
      14  0.35840   0.002  1.000 -0.018 -0.146  0.031  0.011  0.010  0.000 -0.001 -0.000 -0.000 -0.000 -0.000 -0.009  0.034  0.167
      17  0.84434  -0.228 -0.018  1.000 -0.702 -0.465 -0.129 -0.114  0.003  0.015 -0.037  0.024 -0.036  0.019 -0.005  0.008  0.004
      18  0.77752   0.180 -0.146 -0.702  1.000  0.106  0.034  0.036 -0.003 -0.006  0.034 -0.020  0.032 -0.016  0.004 -0.004 -0.023
      19  0.66931   0.060  0.031 -0.465  0.106  1.000 -0.247 -0.153  0.000 -0.022 -0.000 -0.003 -0.002 -0.008  0.007 -0.016 -0.007
      20  0.88771   0.009  0.011 -0.129  0.034 -0.247  1.000  0.869  0.010  0.004  0.002 -0.004  0.002  0.002  0.006  0.003  0.004
      21  0.87430   0.014  0.010 -0.114  0.036 -0.153  0.869  1.000  0.018  0.006  0.009 -0.001  0.003 -0.009  0.012  0.002  0.010
      26  0.81270  -0.007  0.000  0.003 -0.003  0.000  0.010  0.018  1.000  0.053 -0.306  0.133  0.290 -0.110  0.000  0.000  0.000
      27  0.53862   0.035 -0.001  0.015 -0.006 -0.022  0.004  0.006  0.053  1.000 -0.254  0.036 -0.237 -0.021 -0.000  0.000  0.000
      28  0.93181   0.278 -0.000 -0.037  0.034 -0.000  0.002  0.009 -0.306 -0.254  1.000 -0.820  0.730 -0.685  0.000  0.000  0.000
      29  0.86463  -0.353 -0.000  0.024 -0.020 -0.003 -0.004 -0.001  0.133  0.036 -0.820  1.000 -0.713  0.683  0.000  0.000  0.000
      30  0.92780   0.273 -0.000 -0.036  0.032 -0.002  0.002  0.003  0.290 -0.237  0.730 -0.713  1.000 -0.776  0.000  0.000  0.000
      31  0.83556  -0.350 -0.000  0.019 -0.016 -0.008  0.002 -0.009 -0.110 -0.021 -0.685  0.683 -0.776  1.000 -0.000  0.000 -0.000
      36  0.81245   0.001 -0.009 -0.005  0.004  0.007  0.006  0.012  0.000 -0.000  0.000  0.000  0.000 -0.000  1.000 -0.052 -0.298
      37  0.48330  -0.001  0.034  0.008 -0.004 -0.016  0.003  0.002  0.000  0.000  0.000  0.000  0.000  0.000 -0.052  1.000 -0.225
      38  0.90297  -0.000  0.167  0.004 -0.023 -0.007  0.004  0.010  0.000  0.000  0.000  0.000  0.000 -0.000 -0.298 -0.225  1.000
      39  0.82295   0.000 -0.202  0.000  0.006  0.003 -0.004 -0.001  0.000 -0.000  0.000  0.000  0.000 -0.000  0.164  0.064 -0.792
                    1.000 -0.623  0.592
      40  0.90985  -0.000  0.158  0.002 -0.019 -0.005  0.003  0.003  0.000  0.000  0.000  0.000  0.000  0.000  0.388 -0.241  0.638
                   -0.623  1.000 -0.725
      41  0.79832  -0.000 -0.259  0.002  0.020 -0.005 -0.002 -0.008 -0.000  0.000 -0.000 -0.000 -0.000  0.000 -0.133 -0.045 -0.613
                    0.592 -0.725  1.000
```

Summary:

$\tau(B^0) = 453.6 \pm 16.46\ \mu\text{m}$
$r = 1.065 \pm 0.044$

13.2 Systematic uncertainties

We repeat the studies of systematic uncertainties described in section 12 for the new set of variables.

13.2.1 Sample selection

We repeat the combined fit to all available signal Monte Carlo described in section 12.1 and fit for the lifetime ratio. The fit gives $\tau(B^0) = 476.5 \pm 4.6$ μm and $r = 1.030 \pm 0.014$. This result is compatible with the generated value of $r = 1.038$. We assign 0.014 as systematic uncertainty on our measurements in data.

13.2.2 Parameterisation of the resolution function

We repeat the combined fit to all available signal Monte Carlo with two different parameterisations of the resolution function. In both fits the parameters of the resolution function are held fixed and their values are taken from table 8.
We obtain $r = 1.031 \pm 0.012$ using the "G+G" parameterisation, and $r = 1.030 \pm 0.012$ using the "G+G$\otimes$E" parameterisation. We assign the difference of the central values as sytemetic uncertainty on the fitted lifetime ratio obtained using "G+G$\otimes$E".

13.2.3 Identical resolution function

We repeat the study described in section 12.3, fitting for r. On average we obtain $r_{\text{generated}} - r_{\text{reconstructed}} = 0.008 \pm 0.0004$. We assign 0.008 as systematic uncertainty.

13.2.4 Δz outliers

We repeat the fit for r with several combinations of values for the widths of the gaussians that describe Δz outliers for charged and neutral Bs. The results are summarised in table 15.
The uncertainties on r are small if the Δz distributions of B^0 outliers and B^+ outliers are similar. Monte Carlo studies indicate that this is the case. We have already seen that the resolutions functions for the two species are comparable. We assign the value for "2500 $\rightarrow$ 4000, 2500 $\rightarrow$ 3250" (0.005) as systematic uncertainty.

σ gaussian B^0	σ gaussian B^+	change of central value for r
2500 $\rightarrow$ 4000		0.0111
	2500 $\rightarrow$ 4000	0.0123
2500 $\rightarrow$ 4000	2500 $\rightarrow$ 4000	0.0005
2500 $\rightarrow$ 4000	2500 $\rightarrow$ 3250	0.0048

Table 15: Impact of uncertainty on width of outliers gaussians on r.

13.2.5 Detector geometry and alignment

The uncertainty due to the z scale cancels when the ratio of the two lifetimes is calculated.

13.2.6 Boost

The uncertainty from the determination of the average boost cancels in the same way as the uncertainty due to the z scale.
The mass difference between the two species of B mesons is small compared to the energy release in the $\Upsilon(4S)$ decay [1]. Furthermore, the lifetimes of the two species are comparable (see section 10). To a good approximation, the bias due to the average boost approximation will cancel as well. At the present level of precision we neglect any residual effects.

13.2.7 Signal probability

We repeat the variation of parameters from the fit to the substituted mass spectra described in section 12.10. The central value of r changes by 0.0025 (0.0038) if we change the value of the $B^0(B^+)$ signal fraction within 2σ. We assign $\sqrt{0.0025^2 + 0.0038^2} = 0.005$ as systematic uncertainty.

13.2.8 Background modelling

The presence of backgrounds tends to bias both measured lifetimes towards higher values (section 12.11). This bias is significantly larger for charged Bs. To estimate the impact on r we neglect this compensation and take into account only the uncertainty on $\tau(B^+)$. We assign 5.1 μm/ 451.5 μm (see section 12.11) as sytematic uncertainty due to the backgrounds.

13.2.9 Total systematic uncertainty

A summary of all systematic errors as well as their sum (in quadrature) is given in table 16.

systematic effect	uncertainty on r	comment
MC statistics	0.014	
Parameterisation of resolution function	0.001	
One single resolution function	0.008	
Δz outliers	0.005	
z scale	-	cancels
Boost	-	cancels
Signal probability	0.005	
Background modelling	0.011	
Total in quadrature	0.021	

Table 16: Summary of the systematic uncertainties on the lifetime ratio r.

14 Systematic uncertainties (semileptonic events)

15 Conclusions

We add up all uncertainties and apply the corrections mentioned in section 12. The final result reads

$$\begin{aligned} \tau(B^0) &= 451.5 \pm 15.6\ (\text{stat}) \pm 8.8\ (\text{syst})\ \mu\text{m} \\ &= 1.506 \pm 0.052\ (\text{stat}) \pm 0.029\ (\text{syst})\ \text{ps} \end{aligned}$$

$$\begin{aligned} \tau(B^+) &= 480.3 \pm 14.6\ (\text{stat}) \pm 10.6\ (\text{syst})\ \mu\text{m} \\ &= 1.602 \pm 0.049\ (\text{stat}) \pm 0.035\ (\text{syst})\ \text{ps} \end{aligned}$$

$$\frac{\tau(B^+)}{\tau(B^0)} = 1.065 \pm 0.044\ (\text{stat}) \pm 0.021\ (\text{syst})$$

where the first error is statistical (see the discussion in section 12.2) and the second one is sytematic.

A Summary of selection cuts

Reproduce summary tables from BAD 40.

References

[1] Particle Data Group, D.E. Groom *et al.*, "Review of particle physics", Eur. Phys. J. C **15**, 1 (2000).

[2] I. I. Bigi, "Lifetimes of heavy flavor hadrons: whence and whither ?", Nuovo Cim. **109 A**, 713 (1996).

[3] M. Neubert, C. T. Sachrajda, "Spectator effects in inclusive decays of beauty hadrons", Nucl. Phys. B **483**, 339 (1997).

[4] LEP B lifetimes working group. Homepage: http://claires.home.cern.ch/claires/lepblife.html .

[5] R. Kerth *et al.*, "The *BABAR* coordinate system and units", *BABAR* note 230 (1995).

[6] D. Kirkby, "Generator-level studies for $B\overline{B}$ mixing", http://www.slac.stanford.edu/~davidk/BBMix/GenStudy/ , 1999.

[7] P. F. Harrison and H. R. Quinn, eds., "The *BABAR* physics book", SLAC-R-405 (1998), section 11.3.

[8] J. Blouw, A. Soffer and S. Dong, "Measuring the PEP-II boost", *BABAR* analysis document 14 (2000).

[9] The *BABAR* experiment at PEP-II, *BABAR*-PUB-0018, submitted to ICHEP2000.

[10] Breco AWG, "Exclusive B reconstruction to open charm final states", *BABAR* analysis document 40 (2000).

[11] Charmonium AWG, "Exclusive B reconstruction into charmonium final states: status report", *BABAR* analysis document 12 (2000).

[12] Breco AWG, "Selection of D^*-lepton events for B lifetime and mixing analyses", *BABAR* analysis document 34 (2000).

[13] ARGUS collaboration, H. Albrecht *et al.*, "Reconstruction of B mesons", Phys. Lett. **B185**, 218 (1987).

[14] P. Robbe, "Exclusive B reconstruction, Monte Carlo background studies", http://www.slac.stanford.edu/BFROOT/www/Physics/CP/beta/doc/brecoSample/MCBReco.html (2000).

[15] R. Faccini and F. Martínez-Vidal, "Vertexing/kinematic fitting user's guide", http://www.slac.stanford.edu/BFROOT/www/Physics/Tools/Vertex/VtxGuide (2000).

[16] C. de la Vaissière, H. Briand and N. Regnault, "Lifetimes with full B reconstruction", *BABAR* note 436 (1998).

[17] F. Martínez-Vidal, "VtxTagBtaSelFit: a vertex tag reconstruction tool user's guide", http://www.slac.stanford.edu/BFROOT/www/Physics/Tools/Vertex/VtxGuide/VtxTagBtaSelFit.html (2000).

[18] Crystal Ball linse shape function

[19] R. Aleksan, "Quark mixing and *CP* violation", lecture given at NATO-ASI, US Virgin Islands (1998).

[20] J. Stark, "B^0/B^+ lifetimes with fully reconstructed hadronic B decays and the Δz resolution function", April Physics Week (2000).

[21] U. Egede, D. Kirkby and G. Raven, "A user's guide to the `RooFitTools` package for unbinned maximum likelihood fitting", *BABAR* analysis document 18 (2000).

[22] C. Cheng *et al.*, "Beamspot determination and use in *BABAR*", *BABAR* analysis document 13 (2000).

[23] *BABAR* collaboration, D. Boutigny *et al.*, "Technical design report", SLAC-R-95-457 (1995).

[24] J. Schieck, private communication (2000).

[25] G. Raven, "SVT-DCH alignment vs. time", "Design of the tracking reconstruction software" hyper news forum, message 303.

[26] P. Robbe, "Material Interactions", April Physics Week (2000).

[27] C. Hast and P. Robbe, private communication (2000).

[28] E. Charles, private communication (2000).

[29] C. Hast, private communication (2000).

[30] S. Metzler, "Measurement of B lifetimes at *BABAR*", *BABAR* analysis document 65 (2000).

[31] Presentations given at the Forum meeting on May 16^{th} (2000).